JOURNAL OF GEOPHYSICAL RESEARCH, VOL. 105, NO. C10, PAGES 24,119–24,139, OCTOBER 15, 2000

Modeling stratified wave and current bottom boundary layers on the continental shelf

Richard Styles and Scott M. Glenn

Institute of Marine and Coastal Sciences, Rutgers–The State University of New Jersey, New Brunswick, New Jersey

Abstract. The *Glenn and Grant* [1987] continental shelf bottom boundary layer model for the flow and suspended sediment concentration profiles in the constant stress layer above a noncohesive movable sediment bed has been updated. The Reynolds fluxes for sediment mass and fluid momentum are closed using a continuous, time-invariant linear eddy viscosity modified by a continuous stability parameter to represent the influence of suspended sediment–induced stratification throughout the constant stress region. *Glenn and Grant* [1987] use a less realistic discontinuous eddy viscosity and neglect the stratification correction in the wave boundary layer. For typical model parameters the two models produce currents above the wave boundary layer that are in better agreement than the suspended sediment concentrations. Within the wave boundary layer the differences are much greater for both the current and the sediment concentration. This leads to significant differences in the sediment transport throughout the constant stress layer. Sensitivities of the updated model were examined on the basis of observed wave and current data acquired during storms on the inner continental shelf. Comparisons between the stratified and neutral versions of the updated model indicate that the stratified version produces a total depth-integrated sediment transport that can be 2 orders of magnitude less than, and time-averaged shear velocities that can be nearly half of, that predicted by the neutral version. Sensitivities to grain size distributions indicate that even a small amount of finer sediment can stratify the storm-driven flows. Sensitivities to closure constants within the range of reported values also produce up to an order of magnitude variation in sediment transport, illustrating the need for dedicated field experiments to refine further estimates of these parameters.

1. Introduction

Over the past decade a number of independent observational and theoretical studies designed to enhance our present understanding of important physical processes in continental shelf bottom boundary layers have been carried out. Specific areas of advancement include (1) the description of bottom roughness over movable sediment beds [*Wikramanayake and Madsen*, 1991; *Drake et al*., 1992; *Sorenson et al*., 1995; *Xu and Wright*, 1995], (2) the geometrical properties and evolution of wave-formed ripples in the presence of waves or waves and currents [*Wikramanayake and Madsen*, 1991; *Wiberg and Harris*, 1994; *Traykovski et al*., 1999], (3) the relationship between excess boundary shear stress and the entrainment of sediment [*Hill et al*., 1988; *Drake and Cacchione*, 1989; *Vincent and Green*, 1990; *Wikramanayake and Madsen*, 1992; *Madsen et al*., 1993], and (4) the further validation or investigation of simple, commonly employed turbulence closure methods for neutral [*Madsen and Wikramanayake*, 1991; *Wiberg*, 1995] and stratified [*Villaret and Trowbridge*, 1991; *McLean*, 1992] flow regimes. Some of these independent investigations have also produced simple models to describe these processes given a minimal description of the wave, current, and sediment environment. The collective results, however, have not been fully synthesized into a single continental shelf bottom boundary layer model. An improved bottom boundary layer model therefore has been developed to incorporate, either directly or through future validation efforts with field data, the theoretical concepts from some of these studies.

Paper number 2000JC900115.
0148-0227/00/2000JC900115$09.00

The theoretical model presented here is an extension of the *Glenn and Grant* [1987] (hereinafter referred to as GG) stratified bottom boundary layer model. The GG model originally was developed for the constant stress portion of the flow above a noncohesive movable sediment bed. GG adopted the *Grant and Madsen* [1979] turbulence closure scheme and modified the eddy viscosity to include a correction for suspended sediment-induced stratification. Although the GG model incorporates a number of important physical processes such as wave and current interaction and a movable sediment bed, the discontinuous eddy viscosity and stability parameter profiles they use lead to an artificial kink in the current and concentration profiles at the top of the wave boundary layer. The discontinuity will have a strong influence on the model's ability to predict accurately the stratification correction, the velocity and concentration profiles, and therefore the associated sediment transport. Because the bottom stress is related to the product of the flow shear times the eddy viscosity evaluated at the bed, the discontinuity at the top of the wave boundary layer is likely to have less effect on the bottom stress estimates.

An improved continuous eddy viscosity formulation for unstratified flows, which removes the artificial kink in the current and concentration profiles, has been suggested by *Glenn* [1983] and *Madsen and Wikramanayake* [1991] in lieu of the discontinuous form originally proposed by *Smith* [1977] and *Grant and Madsen* [1979]. *Madsen and Wikramanayake* [1991] dem-

onstrated that computed velocity profiles based on the continuous eddy viscosity compared more favorably to velocity profiles obtained from flume data and a numerical model than do profiles based on the *Grant and Madsen* [1986] model. *Wikramanayake and Madsen* [1992] and *Wikramanayake* [1993] extended the *Madsen and Wikramanayake* [1991] wave and current model to include the periodic and mean suspended sediment concentration but did not include suspended sediment–induced stratification. *Lee and Hanes* [1996] incorporated the *Wikramanayake* [1993] model as a modular component of an advective/diffusive model to predict unstratified suspended sediment concentration profiles in the near-shore region off Vilano Beach, Florida. They showed that for high wave conditions the *Wikramanayake* [1993] model was in good agreement with their field observations. *Lynch et al*. [1997] demonstrated that the vertical structure of the mean suspended sediment concentration they measured off the northern California coast was qualitatively similar to profile estimates derived from the *Wikramanayake and Madsen* [1992] model. Therefore several field and laboratory studies have concluded that the improved eddy viscosity model first presented by *Glenn* [1983] and later revisited by *Madsen and Wikramanayake* [1991] and *Wikramanayake and Madsen* [1992] is more accurate in predicting current and concentration profiles than the simpler model developed by *Grant and Madsen* [1979, 1986] for unstratified conditions. This is especially important for sediment transport studies since the horizontal transport is a function of the current and concentration profiles.

All these models more or less stem from earlier versions of the *Grant and Madsen* [1979] bottom boundary layer model, with changes mainly associated with the eddy viscosity formulation; however, less has been done to account for suspended sediment–induced stratification in combined wave and current flows. *Wiberg and Smith* [1983] and GG have treated the case exclusively for the constant stress region. *Wiberg and Smith* [1983] presented two eddy viscosity formulations that included the linear discontinuous form originally presented by *Smith* [1977] and *Grant and Madsen* [1979] and a more complex linear form modified by an exponential decay. Although physically sound, their exponential function requires a numerical solution even when stratification can be neglected. GG used the *Grant and Madsen* [1979] discontinuous eddy viscosity to obtain a simpler solution but neglected the stratification correction within the wave boundary layer. Their decision was based on scaling arguments that demonstrated that for this specific form of the eddy viscosity the stratification correction in the wave boundary layer was small. Because the current and concentration profiles, which depend on the eddy viscosity profile, are coupled through the stratification correction, it is unclear whether the stratification term can be neglected within the wave boundary layer if an alternative eddy viscosity is used. In addition, the stratification correction within the wave boundary layer for a continuous eddy viscosity should also remain continuous if consistency is to be maintained. Therefore the primary purpose here is to revisit the stratification correction and eddy viscosity formulation to improve our modeling capabilities for boundary layer flows and sediment transport on stratified, storm-dominated continental shelves. An additional constraint is to maintain an efficient solution since a primary application is to couple this bottom boundary layer model to existing shelf circulation models [e.g., *Keen and Glenn*, 1994, 1995].

Section 2 presents the theoretical model emphasizing the need for an improved eddy viscosity formulation, the methods used to close the turbulence fluxes for mass and momentum, and the scaling of the stability parameter in the wave boundary layer for a continuous eddy viscosity formulation. This is followed by a comparison between unstratified and stratified versions of the model and an analysis of model sensitivity to sediment grain size distributions and empirically derived model coefficients. Finally, the major results of this study are summarized.

2. Theoretical Model

The theoretical model presented here follows from *Grant and Madsen* [1986] and GG, in which the horizontal (x, y) components of velocity (u, v) are first Reynolds averaged and then divided into independent wave (u_w, v_w) and current (u_c, v_c) contributions, i.e.,

$$\begin{aligned} u &= u_c + u_w + u' \\ v &= v_c + v_w + v', \end{aligned} \tag{1}$$

where u' and v' are the turbulent velocity fluctuations. By further employing the usual boundary layer and linear approximations and assuming a time-independent eddy viscosity the momentum equation is averaged over a wave period to produce the following governing equation for the current:

$$\frac{\tau_c}{\rho} = K \frac{\partial U}{\partial z}, \tag{2}$$

where τ_c is magnitude of the Reynolds stress averaged over a wave period evaluated at the bed, ρ is the fluid density, K is the time-independent eddy viscosity, $U = (u_c^2 + v_c^2)^{1/2}$ is the magnitude of the current, and z is the vertical coordinate measured positive upward from the bed.

For suspended sediment it is customary to assume sediment concentrations are large enough to be treated as a continuum yet small enough to neglect individual particle interactions. To include heterogeneous sediments, GG divided the sediment mixture into distinct phases, each characterized by a unique density and grain size class. By similarly dividing the volumetric concentration (cm^3 of sediment per cm^3 of mixture) into mean (C_{nm}), periodic (C_{np}), and turbulent (c') components,

$$C = C_{nm} + C_{np} + c', \tag{3}$$

for each size/density class n and applying conservation of mass to each class, the equations governing the mean concentrations become

$$w_{f_n} \frac{\partial C_{nm}}{\partial z} + \frac{\partial}{\partial z}\left(K_s \frac{\partial C_{nm}}{\partial z} \right) = 0, \tag{4}$$

where w_{f_n} is the particle-settling velocity for each class and K_s is the eddy diffusivity for suspended sediment. Equation (4) is the well-known relationship describing an equilibrium sediment concentration profile where the upward turbulent flux of sediment is balanced by gravitational settling.

2.1. Eddy Viscosity

Grant and Madsen [1979] suggest the following simple, two-layer eddy viscosity to close the fluid momentum equation:

$$\begin{aligned} K &= \kappa u_{*cw} z, \qquad z \le \delta_w, \\ K &= \kappa u_{*c} z, \qquad z > \delta_w, \end{aligned} \tag{5}$$

where κ is von Karman's constant (0.4), $u_* = \sqrt{\tau/\rho}$ is the shear velocity, τ is the magnitude of the shear stress, and δ_w is the wave boundary layer height. The characteristic shear velocity within the wave boundary layer, u_{*cw}, is written in terms of the maximum shear stress for the wave plus the current [*Grant and Madsen*, 1979]. Outside the wave boundary layer the shear stress is associated with the time-averaged current only, so the characteristic shear velocity, u_{*c}, is derived from the time-averaged current.

One weakness in the *Grant and Madsen* [1979] and GG models is a discontinuity in the eddy viscosity at the top of the wave boundary layer. Previous work for the pure wave case can help define an alternative formulation that is continuous. *Grant and Madsen* [1986] presented a comparison between modeled and measured profiles of the maximum wave velocity and phase in an oscillatory boundary layer. Their results indicate that an eddy viscosity that increases linearly throughout the wave boundary layer is less accurate than one that starts off linearly increasing near the bed, but then decays, through an exponential modulation, as the top of the wave boundary layer is approached. Their results are consistent with oscillatory boundary layers in which a transition region exists that separates the log layer near the bed from the potential flow region above the wave boundary layer. In the transition region the magnitude of the wave shear is weakening, with a corresponding reduction in the production of turbulent kinetic energy (TKE). The exponential modulation used by *Grant and Madsen* [1986] reduces the value of the eddy viscosity in the transition region in accordance with the reduction in TKE production. The much larger linearly increasing eddy viscosity, on the other hand, overestimates the turbulent transport in the transition region and leads to the poorer comparison between the magnitude of the velocity profile and phase demonstrated by *Grant and Madsen* [1986]. On the basis of the wave data of *Jonsson and Carlsen* [1976], *Nielsen* [1992] constructed an eddy viscosity profile that also revealed a structure similar to the linear exponential form. A linear eddy viscosity modulated by an exponential decay has been suggested to model combined flows as well [*Wiberg and Smith*, 1983; *Glenn*, 1983; GG]. An analytical solution to the governing equations, however, is not possible using a linear eddy viscosity modified by an exponential decay.

As an intermediate alternative, continuous eddy viscosity profiles that are linearly increasing near the bed and then constant in the transition region have been proposed. Because the exponential modulation is weak for small z, the linearly increasing eddy viscosity is similar to the linear exponential form near the bed. In the transition region the linear exponential decay formulation smoothly reaches a maximum. In the vicinity of the maximum the linear exponential decay formulation can be approximated by a constant eddy viscosity. For a wave boundary layer embedded within a larger current boundary layer the production of TKE due to the current shear can still be significant above δ_w. In this region a linearly increasing eddy viscosity is appropriate if the characteristic velocity scale is altered to include only the contribution from the time-averaged shear stress. For this study the following three-layer eddy viscosity profile is chosen as it combines the formulation for the pure wave case with a combined wave and current boundary layer:

$$K = \kappa u_{*c} z, \qquad z_2 < z,$$

$$K = \kappa u_{*cw} z_1, \qquad z_1 < z \le z_2, \tag{6}$$

$$K = \kappa u_{*cw} z, \qquad z_0 \le z \le z_1,$$

where z_0 is the hydrodynamic roughness, z_1 is an arbitrary scale that defines the lower boundary of the transition layer, and $z_2 = z_1 u_{*cw}/u_{*c}$, which is determined by matching the eddy viscosities at $z = z_2$. Similar to the *Grant and Madsen* [1979] eddy viscosity model, the characteristic velocity scales within and above the wave boundary layer are u_{*cw} and u_{*c}, respectively. To remove the discontinuity, an additional layer is inserted between the inner and outer layers that scales with u_{*cw} and the length scale z_1. The eddy viscosity in this transition region reflects the contribution to the stress by the combined flow while ensuring that the decrease in turbulence transport associated with the wave is represented through the constant length scale z_1, rather than the linearly increasing length scale z. The three-layer eddy viscosity model for this application was first proposed by *Glenn* [1983] and later revisited by *Madsen and Wikramanayake* [1991].

2.2. Stability Parameter

The effects of vertical stratification on the momentum balance are expressed through a modification to the neutral eddy viscosity,

$$K_{\text{strat}} = \frac{K}{1 + \beta \dfrac{z}{L}}, \tag{7}$$

with a similar modification for the turbulent diffusion of sediment mass,

$$K_{s\ \text{strat}} = \frac{K}{\gamma + \beta \dfrac{z}{L}}, \tag{8}$$

where γ and β are constants, L is the Monin-Obukov length, and the ratio z/L is the stability parameter described below (GG). On the basis of estimates obtained from thermally stratified flows in the atmospheric boundary layer [*Businger et al.*, 1971], GG adopt values of $\gamma = 0.74$ and $\beta = 4.7$. Even though similarity arguments suggest that the stratified flow analogy is valid for continental shelf bottom boundary layers, caution must be used when assuming that empirically determined coefficients derived for thermally stratified flows in air will apply to flows stratified by suspended sediment in water. *Villaret and Trowbridge* [1991] addressed this issue by comparing previously reported laboratory measurements of suspended sediment concentration and current profiles with a theoretical model that incorporates the effects of suspended sediment–induced stratification in a similar manner as presented here. They found the stratified flow analogy for suspended sediment–induced stratification was valid for the steady current and concentration data they examined and that empirically derived coefficients were consistent with what had been reported for thermally stratified atmospheric boundary layers. As was done by *Wiberg and Smith* [1983] and GG, a neutral eddy viscosity modulated by a buoyancy term is assumed to remain a valid and useful approximation to describe the first-order effects of suspended sediment–induced stratification in a combined wave and current boundary layer.

Following *Stull* [1988], the Richardson flux number for horizontally homogeneous flow can be defined by

$$R_f = \frac{\frac{g}{\bar{\rho}}\overline{\rho' w'}}{\overline{u'w'}\frac{\partial \bar{U}}{\partial z} + \overline{v'w'}\frac{\partial \bar{V}}{\partial z}} = \frac{K_{\text{strat}}}{u_*^4}\frac{g}{\bar{\rho}}\overline{\rho' w'}, \tag{9}$$

where g is the acceleration due to gravity, $\bar{\rho}$ is the Reynolds averaged density, ρ' is the turbulent density fluctuation, $\bar{U}$ and $\bar{V}$ are the horizontal components of the Reynolds averaged velocity, w' is the vertical component of the turbulent velocity fluctuations, and u_* is a to-be-determined characteristic shear velocity. The terms $\overline{u'w'}$ and $\overline{v'w'}$ are the familiar horizontal components of the Reynolds stress, and $\overline{\rho' w'}$ is the Reynolds flux for sediment mass. The second equality in (9) indicates that the stratified eddy viscosity has been used to eliminate the vertical shear. The Richardson flux number is related to the stability parameter by $R_f = (K_{\text{strat}}/K)(z/L)$ [*Turner*, 1979]. Using this relation and (9), the stability parameter becomes

$$\frac{z}{L} = \frac{K}{u_*^4}\frac{g}{\bar{\rho}}\overline{\rho' w'}. \tag{10}$$

In the constant stress layer it is assumed that temperature and salinity are well mixed so that the only source of flow stratification is suspended sediment. Following *Glenn* [1983], ρ' and $\bar{\rho}$ can be expressed in terms of the sediment concentration, giving

$$\rho' = \rho \sum_{n=1}^{N} (s_n - 1) c_n' \tag{11}$$

$$\bar{\rho} = \rho\left[1 + \sum_{n=1}^{N} (s_n - 1)\overline{C_n}\right] \simeq \rho, \tag{12}$$

where N is the total number of sediment size/density classes, $\overline{C_n}$ is the Reynolds averaged concentration ($\overline{C_n} = C_{nm} + C_{np}$), and $s_n = \rho_{sn}/\rho$, (ρ_s = sediment density) is the relative sediment density for each size/density class n. Substituting (11) and (12) into (10), the stability parameter becomes

$$\frac{z}{L} = \frac{K}{u_*^4}\sum_{n=1}^{N} g(s_n - 1)\,\overline{c_n' w'}. \tag{13}$$

Rewriting (13) using the stratified eddy diffusivity to represent the Reynolds flux for sediment mass results in the following expression for the stability parameter:

$$\frac{z}{L} = -\frac{K}{u_*^4}\sum_{n=1}^{N} g(s_n - 1) K_{s\,\text{strat}}\frac{\partial \overline{C_n}}{\partial z}. \tag{14}$$

2.3. Wave Friction Factor and the Determination of the Bottom Stress

As mentioned above, the maximum instantaneous shear stress for the combined flow is the vector sum of the time average of the instantaneous shear stress, $\boldsymbol{\tau}_\mathbf{c}$, plus the maximum shear stress associated with the wave, $\boldsymbol{\tau}_\mathbf{wm}$:

$$\boldsymbol{\tau}_\mathbf{cw} = \boldsymbol{\tau}_\mathbf{c} + \boldsymbol{\tau}_\mathbf{wm}, \tag{15}$$

where boldface denotes a vector. Writing (15) in terms of the shear velocities and taking the magnitude gives

$$u_{*cw}^2 = C_R u_{*wm}^2, \tag{16}$$

where

$$C_R = \left[1 + 2\left(\frac{u_{*c}}{u_{*wm}}\right)^2 \cos\boldsymbol{\phi}_{cw} + \left(\frac{u_{*c}}{u_{*wm}}\right)^4\right]^{1/2}, \tag{17}$$

$\boldsymbol{\phi}_{cw}$ ($0° \le \boldsymbol{\phi}_{cw} \le 90°$) is the angle between the current and the wave, and the x axis has been aligned to coincide with τ_{wm} [*Grant and Madsen*, 1986].

As has been done in the past, the calculation of the bed shear stress is simplified by introducing a wave and current friction factor f_{cw} that relates the magnitude of the maximum shear stress for the wave, τ_{wm}, to the magnitude of the near-bed orbital velocity, u_b:

$$\tau_{wm} = \frac{1}{2} f_{cw} C_R \rho u_b^2, \tag{18}$$

where the effect of the enhanced current is expressed through C_R [*Grant and Madsen*, 1986]. When $u_{*c} \to 0$, $C_R \to 1$ and (18) produces the usual expression for the shear stress for pure wave motion. As C_R increases, τ_{wm} becomes larger, representing the enhancement of the wave stress by the time-averaged current.

The magnitude of the maximum shear stress for the wave under neutral conditions can also be expressed as

$$\tau_{wm} = \lim_{z \to z_0}\left(\rho K\left|\frac{\partial u_w}{\partial z}\right|\right), \tag{19}$$

where $|\ |$ denotes the modulus. Equation (19) can be simplified by introducing the nondimensional wave shear

$$\Gamma_{cw} \equiv \frac{1}{u_b}\lim_{\xi \to \xi_0}\left(\left|\frac{\partial u_w}{\partial \xi}\right|\right), \tag{20}$$

where $\xi = z/l_{cw}$ is the nondimensional vertical coordinate, $l_{cw} = \kappa u_{*cw}/\omega$ is the scale height of the wave boundary layer, ω is the wave radian frequency, and $\xi_0 = z_0/l_{cw}$ is the nondimensional hydraulic roughness. Γ_{cw} can be derived from the solution to the wave shear, which is presented in Appendix A. Introducing (20) into (19) and substituting the neutral eddy viscosity from (6) gives

$$\frac{\tau_{wm}}{\rho} = \kappa \xi_0 u_{*cw} u_b \Gamma_{cw}. \tag{21}$$

By substituting (21) into (18) and using (16), an alternative expression for the wave friction factor can be derived:

$$\frac{f_{cw}}{2} = (\kappa \xi_0 \Gamma_{cw})^2. \tag{22}$$

Inspection of the terms that define Γ_{cw} (see Appendix A) shows that f_{cw} is only a function of the nondimensional parameters ξ_0, $\xi_1 = z_1/l_{cw}$, $\xi_2 = z_2/l_{cw}$, and $\varepsilon = u_{*cw}/u_{*c}$. Because the eddy viscosity profile is continuous, we have the additional constraint that $\xi_2 = \xi_1 \varepsilon$, leaving only three independent parameters, ξ_0, ξ_1, and ε. The first two can be simplified further.

Using the Nikuradse equivalent sand grain roughness, z_0 can be written as

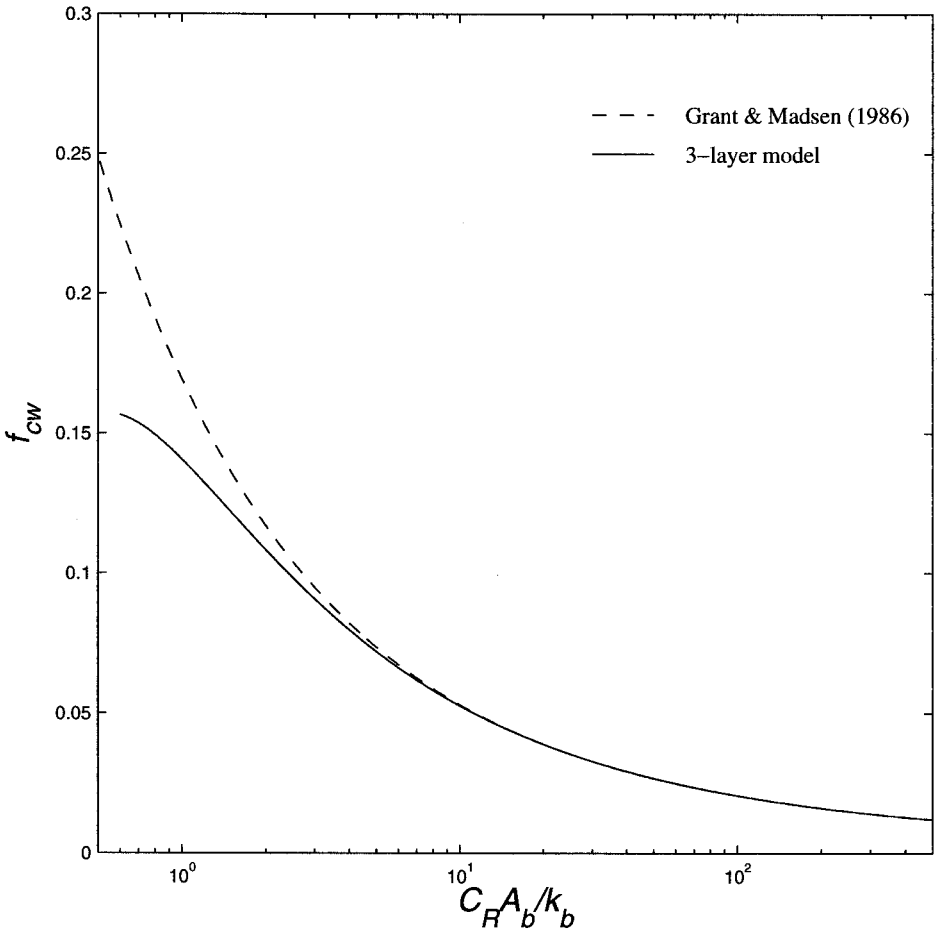

Figure 1. Comparison of the combined wave and current friction factor calculated using the three-layer model developed for this study and the *Grant and Madsen* [1986] model.

$$z_0 = \frac{k_b}{30}, \tag{23}$$

where k_b is the physical bottom roughness length. Using (23), along with (16) and (18), the equation for ξ_0 becomes

$$\xi_0 = \frac{k_b}{30 l_{cw}} = \frac{k_b}{30\kappa\sqrt{f_{cw}/2}\, C_R A_b}, \tag{24}$$

where $A_b = u_b/\omega$ is the near-bottom excursion amplitude of the wave motion. This indicates that the nondimensional roughness length ξ_0 is a function of f_{cw} and $k_b/C_R A_b$.

In the past the height z_1 has been specified as a constant times the scale height of the wave boundary layer ($z_1 = \alpha l_{cw}$). Experimental values for α span an order of magnitude ranging from 0.15 for waves in a laboratory flume [*Madsen and Wikramanayake*, 1991] to 2.0 based on sediment concentration profiles measured in the field [*Lynch et al*., 1997]. Since the purpose here is to examine the quantitative features of a theoretical bottom boundary layer model, α will remain a free parameter and its sensitivities will be investigated. The nondimensional height ξ_1 is now equal to α, which gives $\xi_2 = \xi_1\varepsilon = \alpha\varepsilon$. The friction factor in (22) now becomes a function of $k_b/C_R A_b$, α, and ε. This is different from the friction factor derived from the *Grant and Madsen* [1986] two-layer eddy viscosity model, where f_{cw} is only a function of the first nondimensional parameter $k_b/C_R A_b$.

Figure 1 shows f_{cw} as a function of $C_R A_b/k_b$ for $\varepsilon = 2.1$ and $\alpha = 0.5$ and shows the *Grant and Madsen* [1986] wave friction factor for comparison. The value $\alpha = 0.5$ has been suggested by *Madsen and Wikramanayake* [1991] for modeling currents in the presence of waves, and $\varepsilon = u_{*cw}/u_{*c} = 2.1$ represents an intermediate value where the magnitude of the wave and current velocities outside the wave boundary layer are similar. The friction factors derived from both models are the same for large values of $C_R A_b/k_b$ but then diverge as $C_R A_b/k_b$ approaches unity. *Grant and Madsen* [1982], in a study of bottom roughness associated with oscillatory, fully rough turbulent flow, hypothesized that for $A_b/k_b \leq 1$ the proper length scale for the turbulent eddies becomes A_b and not k_b. In this limit, f_{cw} is assumed to be constant and equal to the value obtained by setting $A_b/k_b = 1$ (0.23 for pure waves). Unlike that by *Grant and Madsen* [1982], the friction factor from the three-layer eddy viscosity for combined flows is self limiting, approaching a value of about 0.16 when $C_R A_b/k_b$ is O(1).

As previously mentioned, f_{cw} also is a function of the additional parameters $\alpha = z_1/l_{cw}$ and $\varepsilon = u_{*cw}/u_{*c}$. Figure 2a shows f_{cw} for varying ε and $\alpha = 0.5$, and Figure 2b shows the same but with $\varepsilon = 2.1$ and varying α. The solutions are only weakly dependent on changes in ε, except when $C_R A_b/k_b$ is less than about 1.0, in which case smaller ε tends to produce higher f_{cw}. For $C_R A_b/k_b > 10$ the effect of changing α appears minimal for the $\alpha = 0.5$ and 1.0 cases (Figure 2b). As this

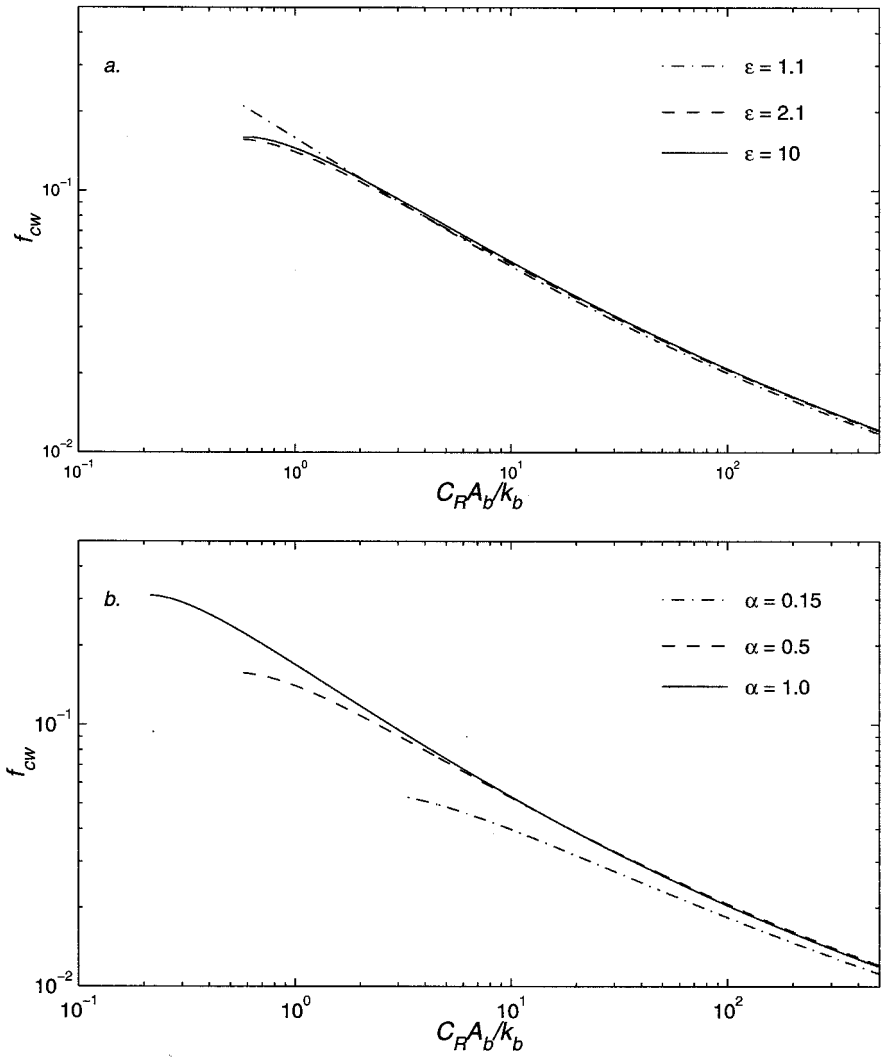

Figure 2. Sensitivity test showing the wave friction factor calculated using the three-layer model as a function of the parameters (a) ε and (b) α. In Figure 2a, $\alpha = 0.5$, and in Figure 2b, $\varepsilon = 2.1$.

ratio decreases, f_{cw} steers toward a constant in agreement with *Grant and Madsen*'s [1982] suggestion that f_{cw} approaches a constant value for large roughness configurations. As $C_R A_b/k_b$ decreases even further, the ratio z_1/z_0 approaches one. For z_1 less than z_0 the three-layer eddy viscosity is no longer valid. This may occur when large ripples produce large values of z_0 that eliminate the lower layer. Since we are primarily interested in modeling storm sediment transport, where near-bed wave velocities will wash out the large ripples, our concern here is the three-layer solution.

Grant and Madsen [1986] derived their wave friction factor solution without examining the sensitivity of C_R to different wave and current conditions. Recalling that $\varepsilon = u_{*cw}/u_{*c}$, (16) is substituted into (17), giving

$$(1 - \varepsilon^4)C_R^2 + 2\cos\phi_{cw}\varepsilon^2 C_R + \varepsilon^4 = 0, \tag{25}$$

which is quadratic in C_R with the solution

$$C_R = \frac{-\cos\phi_{cw}\varepsilon^2 - \sqrt{\cos^2\phi_{cw}\varepsilon^4 - (1 - \varepsilon^4)\varepsilon^4}}{(1 - \varepsilon^4)}. \tag{26}$$

Since $\varepsilon > 1$, the minus is chosen to ensure that C_R is positive. A three-dimensional mesh plot showing the dependence of C_R on ε and ϕ_{cw} is depicted in Figure 3. When ε is large, τ_{wm} constitutes a major fraction of the total shear stress so that C_R is a minimum. As ε approaches 1, $C_R \to \infty$, which means that the contribution to the combined stress from τ_{wm} is negligible and the solution approaches that of a pure current. Examining how C_R varies with ϕ_{cw} for small values of ε is also interesting. When $\varepsilon = 1.5$, which corresponds to the lower limit in Figure 3, C_R varies between 1.1 for $\phi_{cw} = 90°$ and 1.8 for $\phi_{cw} = 0°$. Thus, when the current stress is similar to the maximum wave stress, accurate estimates of ϕ_{cw} are more important. For larger values of ε (large waves) the solution for C_R is much less dependent on the relative direction between the wave and current, and accurate estimates of ϕ_{cw} are not as crucial.

2.4. Solution for the Current and Suspended Sediment Concentration

Substituting the stratified eddy viscosity and the shear velocity into (2), the governing equation for the current magnitude becomes

$$u_{*c}^2 = K_{\text{strat}}\frac{\partial U}{\partial z}. \tag{27}$$

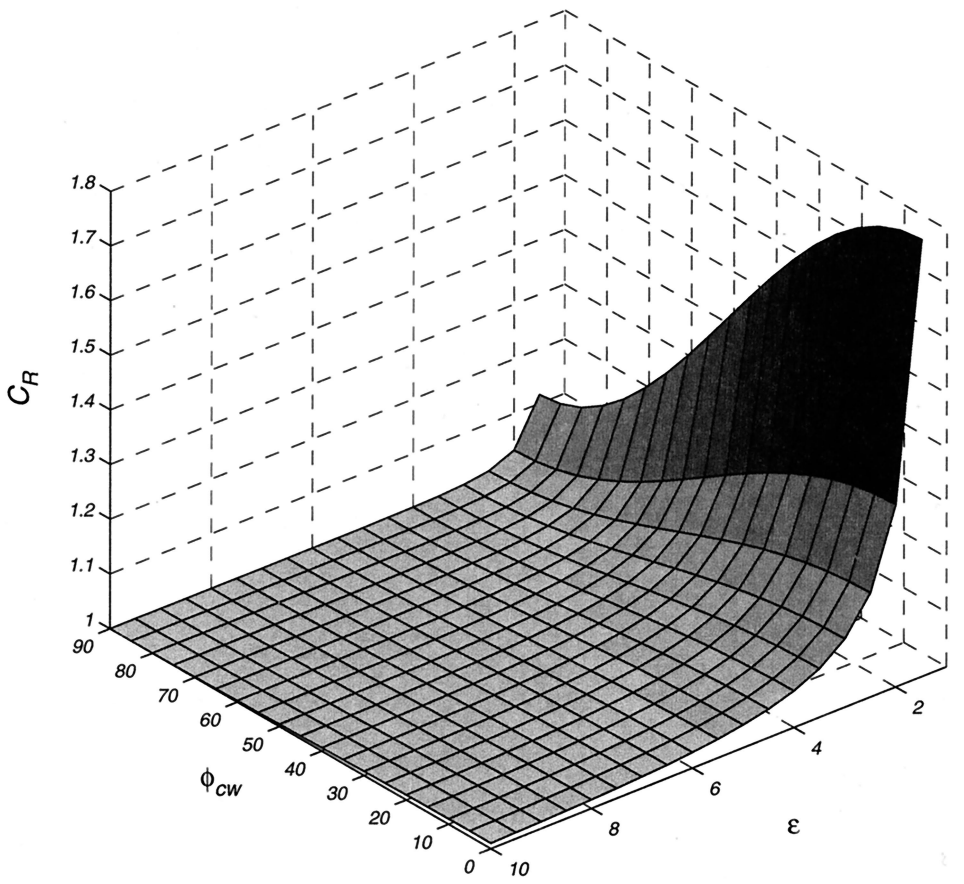

Figure 3. Three-dimensional gridded mesh plot showing C_R as a function of ε and ϕ_{cw}, where ε ranges from a minimum of 1.5 to a maximum of 10 and the grid is spaced in increments of $\frac{1}{2}$ for ε and 5° for ϕ_{cw}.

Using (6) for the neutral portion of the eddy viscosity in each of the three layers and (7) for K_{strat}, (27) is integrated to give

$$U(z) = \frac{u_{*c}}{\kappa}\left[\ln\left(\frac{z}{z_2}\right) + \beta\int_{z_2}^{z}\frac{dz}{L}\right] + U(z_2), \qquad z_2 < z,$$

$$U(z) = \frac{u_{*c}^2}{\kappa u_{*cw}}\left[\frac{(z-z_1)}{z_1} + \frac{\beta}{z_1}\int_{z_1}^{z}\frac{z}{L}\,dz\right] + U(z_1), \qquad z_1 < z \le z_2, \tag{28}$$

$$U(z) = \frac{u_{*c}^2}{\kappa u_{*cw}}\left[\ln\left(\frac{z}{z_0}\right) + \beta\int_{z_0}^{z}\frac{dz}{L}\right], \qquad z_0 \le z \le z_1,$$

where the boundary condition $U(z_0) = 0$ has been imposed along with the requirement that $U(z)$ is continuous at z_1 and z_2.

For the mean suspended sediment concentration, (4) is vertically integrated to give

$$w_{f_n}C_{nm} + K_{s\ \text{strat}}\frac{\partial C_{nm}}{\partial z} = \text{const}, \tag{29}$$

where $K_{s\ \text{strat}}$ has been substituted for K_s and the constant is set equal to zero since at the top of the boundary layer there is no upward turbulent flux out of the boundary layer and no sediment falling downward from above. Using (6) to represent the neutral portion of the eddy viscosity in $K_{s\ \text{strat}}$, the solution for the mean concentration given in (29) becomes

$$C_{nm}(z) = C_{nm}(z_2)\left(\frac{z}{z_2}\right)^{-\gamma w_{f_n}/\kappa u_{*c}}\exp\left[\frac{-\beta w_{f_n}}{\kappa u_{*c}}\int_{z_2}^{z}\frac{dz}{L}\right], \qquad z_2 < z,$$

$$C_{nm}(z) = C_{nm}(z_1)e^{-\gamma w_{f_n}(z-z_1)/\kappa u_{*cw}z_1}\exp\left[\frac{-\beta w_{f_n}}{\kappa u_{*cw}z_1}\int_{z_1}^{z}\frac{z}{L}\,dz\right], \qquad z_1 < z \le z_2, \tag{30}$$

$$C_{nm}(z) = C_{nm}(z_0)\left(\frac{z}{z_0}\right)^{-\gamma w_{f_n}/\kappa u_{*cw}}\exp\left[\frac{-\beta w_{f_n}}{\kappa u_{*cw}}\int_{z_0}^{z}\frac{dz}{L}\right], \qquad z_0 \le z \le z_1,$$

where the concentration at the lower boundary, $C_{nm}(z_0)$, equals an independently prescribed reference value and the requirement that the solution be continuous at z_1 and z_2 has been imposed.

The current profile in (28) is controlled by the two terms appearing in square brackets. The first term represents the neutral solution, where the z dependence is described by a logarithmic function in the inner and outer layers and a linear function in the transition layer. The neutral solution is identi-

cal to that obtained by *Glenn* [1983] and *Madsen and Wikramanayake* [1991]. The second term represents the correction for suspended sediment–induced stratification, where the vertical variation is regulated by the integral of $1/L$ in the inner and outer layers and by the integral of z/L in the transition layer. This is different from the GG model, which neglects the stability parameter in the wave boundary layer. For the special case when z/L is constant the vertical dependence for the current remains logarithmic in the inner and outer layers and linear in the transition layer. This behavior for the log layer was also demonstrated by GG for the two-layer eddy viscosity model.

The concentration equation in (30) is also modulated by two factors representing neutral and stratified solutions. The middle factor on the right-hand side of (30) represents the neutral solution, where a classic Rouse-like profile in the inner and outer layers is separated by an exponential decay in the transition layer. This is similar to the concentration profile obtained by *Glenn* [1983] and *Wikramanayake and Madsen* [1992]. The final exponential factor represents the stratification correction. Like the current, the vertical dependence of the stratified solution is the same as the neutral solution only when z/L is constant.

2.5. Determination of the Stability Parameter

Examination of the stability parameter given in (14) shows that the buoyancy-related term is a function of the Reynolds averaged concentration gradient, which depends on both the mean and periodic concentration. In the transition layer and above, the periodic concentration gradient is an order of magnitude less than the mean concentration gradient [*Glenn*, 1983]. Even though the stability parameter is large enough to affect the current solution in this region, the effect of the periodic concentration gradient is negligible. On the basis of the assumption that the Reynolds averaged concentration evaluated at the bed is a function of the absolute value of the instantaneous shear stress, *Glenn* [1983] concluded that the boundary condition for the periodic concentration within the wave boundary layer could not be expressed as a simple periodic function of time and must be solved numerically. Within the inner layer the periodic concentration gradient can be the same order of magnitude as the mean concentration gradient. However, the stability parameter will be small simply because of the smallness of z and will have little effect on the current and mean sediment concentration solutions. Without including the periodic concentration the stability parameter in (14) reduces to

$$\frac{z}{L} = -\frac{K}{u_*^4}\sum_{n=1}^{N} g(s_n - 1)K_s\frac{\partial C_{nm}}{\partial z}. \tag{31}$$

By substituting (29) into (31) the alternative expression

$$\frac{z}{L} = \frac{K}{u_*^4}\sum_{n=1}^{N} g(s_n - 1)w_{fn}C_{nm} \tag{32}$$

is obtained. The remaining step is to obtain appropriate representations for the characteristic shear velocity in each of the three layers defined by the eddy viscosity profile.

The modulus of the theoretical wave velocity derived in Appendix A and the associated wave shear are functions of the vertical coordinate. Because the modulus of the wave shear remains inversely proportional to z only in the limit where z goes to z_0, the product of the eddy viscosity and the wave shear is not constant throughout the wave boundary layer. This means that the maximum wave shear stress τ_w will also be a function of z even though the time-averaged shear stress is constant. The maximum shear velocity for the combined flow at any level z is related to τ_w and current stress components by

$$u_*^2 = \frac{1}{\rho}|\tau_c + \tau_w| \simeq \frac{1}{\bar{\rho}}|\tau_c + \tau_w|. \tag{33}$$

Writing the stresses in (33) in terms of their respective shear velocities and taking the magnitude gives

$$u_*^2 = \sqrt{u_{*c}^4 + 2u_{*c}^2u_{*w}^2\cos\boldsymbol{\Phi}_{cw} + u_{*w}^4}. \tag{34}$$

The time-averaged shear velocity u_{*c} is constant over the constant stress layer, so that the problem of finding the characteristic shear velocity to define the stability parameter is reduced to obtaining an appropriate expression for the shear velocity for the wave. This is determined through a gradient transport relation that relates the product of the eddy viscosity and the wave shear to the wave stress.

Using the nondimensional coordinate $\xi = z/l_{cw}$, the small argument approximation to the Kelvin functions given by *Abramowitz and Stegun* [1964] can be used to determine the wave solution in the range $\xi < \xi_1$:

$$u_w = u_b + \bar{A} - \frac{\bar{B}}{2}\left(\ln\xi + 1.154 + i\frac{\pi}{2}\right), \tag{35}$$

where $\bar{A}$ and $\bar{B}$ are complex constants [*Grant*, 1977]. Taking the derivative of (35) with respect to ξ gives the wave shear,

$$\frac{\partial u_w}{\partial\xi} = -\frac{\bar{B}}{2\xi}, \tag{36}$$

which when multiplied by the eddy viscosity ($K = \kappa u_{*cw}\xi l_{cw}$) shows that the wave shear stress is constant and equals the maximum bed shear stress for the wave, $\tau_{wm} = \rho u_{*wm}^2$. Thus for $\xi < \xi_1$ the wave shear velocity is approximated by u_{*wm}. With this substitution, $u_*^2 = u_{*cw}^2$. For $\xi > \xi_2$ the shear stress associated with the wave is negligible and the stress for the current is still constant. In this region, $u_*^2 = u_{*c}^2$. Therefore the characteristic velocity scales for the inner and outer layers are identical to those originally adopted by GG.

In the transition region ($\xi_1 < \xi < \xi_2$) the neutral eddy viscosity that defines the stability parameter in (32) is constant ($K = \kappa u_{*cw}l_{cw}\xi_1$). If u_{*cw} is chosen as the characteristic velocity scale, then the production-related term u_*^4/K is equal to $u_{*cw}^3/\kappa z_1$. This is the same as the production-related term for the inner layer evaluated at z_1, so the stability parameter is continuous at z_1. By substituting z_2 for z_1u_{*cw}/u_{*c}, the production-related term in the transition region can alternatively be written $u_{*cw}^4/\kappa u_{*c}z_2$. The production-related term in the outer layer evaluated at z_2 is $u_{*c}^3/\kappa z_2$, which indicates that the production-related term and hence the stability parameter in the transition region are discontinuous at z_2. By the same method, if u_{*c} is chosen as the characteristic velocity scale, then the production-related term in the transition region can be written $u_{*c}^3/\kappa z_2$ and the stability parameter will be continuous at z_2 but discontinuous at z_1. Because one of the goals of this study is to maintain a continuous stratified eddy viscosity, an alternative characteristic shear velocity is selected to ensure

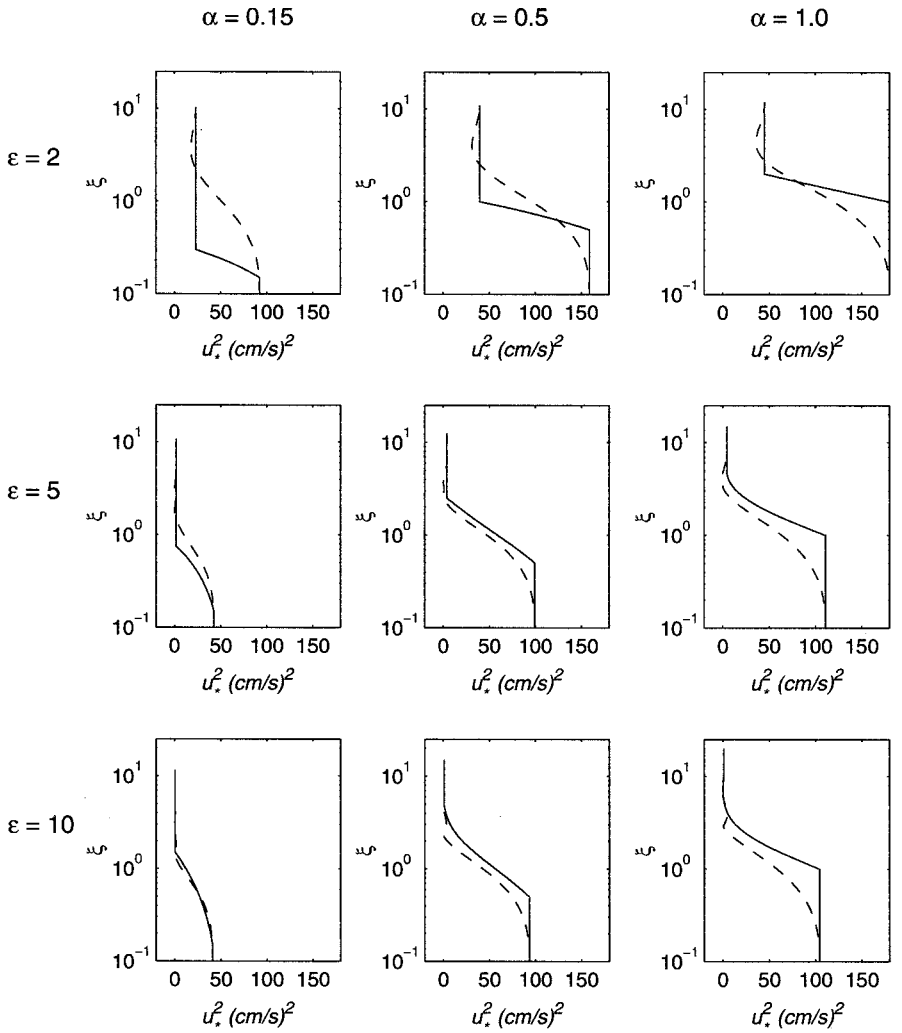

Figure 4. Comparison between the characteristic shear velocity defined in (38) (solid) and the exact solution (dashed) derived using the theoretical wave shear stress. The rows correspond to advancing ε, and the columns correspond to advancing α.

the production-related term and the associated stability parameter remain continuous across the transition region.

For the transition region, ξ is no longer small and it is no longer valid to use the small argument approximation to the Kelvin functions to obtain the solution for the wave. A formal approach would be to solve explicitly for the wave stress and to substitute the values into (34). This approach, however, is not in the spirit of the original goal of developing a simple model that can be efficiently applied at every grid point in a three-dimensional shelf circulation model. An approach that is consistent with this goal and preserves the wave contribution to the total stress to first order is approximating u_*^2 in the region $\xi_1 \le \xi \le \xi_2$ using a function that maintains the general functional form of the wave stress but with a much simpler expression that can be prescribed independent of the details of the wave solution. Inspection of the wave solution in the range $\xi_1 \le \xi \le \xi_2$ (equation (A17)) can be used to show that the vertical decay for the wave shear is exponential. Maintaining an exponential form for the ξ dependence, the characteristic shear velocity in the range $\xi_1 \le \xi \le \xi_2$ is approximated by

$$u_*^2 \simeq c_1 e^{\xi} + c_2 e^{-\xi}, \tag{37}$$

with the boundary conditions $u_*^2 = u_{*cw}^2$ at $\xi = \xi_1$ and $u_*^2 = u_{*c}^2$ at $\xi = \xi_2$. Using these boundary conditions to compute the constants in (37), u_*^2 becomes

$$u_*^2 \simeq u_{*t}^2 = \frac{u_{*c}^2 \sinh(\xi - \xi_1) + u_{*cw}^2 \sinh(\xi_2 - \xi)}{\sinh(\xi_2 - \xi_1)}, \qquad \xi_1 < \xi < \xi_2, \tag{38}$$

where u_{*t} is now the characteristic shear velocity representing the wave stress in the transition region. At $\xi = \xi_1$, u_{*t}^2 equals u_{*cw}^2; u_{*t}^2 then continuously decays to u_{*c}^2 at $\xi = \xi_2$.

The exact solution to the wave shear will depend on the parameters α and ε, which influence ξ_1 and ξ_2. Figure 4 is a matrix of plots depicting u_*^2 calculated from the exact wave solution presented in Appendix A and the approximation (38) for $\varepsilon = 2$, 5, and 10 (increasing influence of the wave) and $\alpha = 0.15$, 0.5, and 1.0 (increasing inner layer thickness). For $\varepsilon = 2$ the departure of the approximation from the exact solution is greatest in the outer layer when $\alpha = 0.15$. The departure from the exact solution is similarly large near the bed when $\alpha = 1.0$. For $\varepsilon = 5$ the match between the exact solution and the

approximation is improved for all α. For $\varepsilon = 10$ the comparison is further improved for $\alpha = 0.15$. In addition, the form of the approximate solution in response to changes in α possesses a distinct pattern at the extremes ξ_1 and ξ_2. For $\alpha = 0.15$ and $\varepsilon = 5$ or 10 the approximate solution is more smooth at $\xi = \xi_1$ and more kinked at $\xi = \xi_2$. For $\alpha = 1.0$ the pattern is reversed. In all nine cases, the wave shear stress approaches a constant near the bed, supporting the use of u_{*wm} to represent the characteristic shear velocity for the wave in (34) when $\xi < \xi_1$.

The stability parameter in each of the three layers can now be written in terms of z as

$$\frac{z}{L} = \frac{K}{u_{*c}^4} \sum_{n=1}^{N} g(s_n - 1) w_{f_n} C_{nm}, \qquad z_2 < z,$$

$$\frac{z}{L} = \frac{K}{u_{*t}^4} \sum_{n=1}^{N} g(s_n - 1) w_{f_n} C_{nm}, \qquad z_1 < z \le z_2, \tag{39}$$

$$\frac{z}{L} = \frac{K}{u_{*cw}^4} \sum_{n=1}^{N} g(s_n - 1) w_{f_n} C_{nm}, \qquad z_0 \le z \le z_1.$$

Utilizing (38) to represent the characteristic shear velocity in the transition region not only preserves the contribution from the wave to the total but also insures that z/L, and therefore the stratified eddy viscosity, remains continuous throughout the constant stress layer.

GG chose to neglect the stability parameter in the wave boundary layer on the basis of a systematic scaling analysis that showed z/L was at most $O(10^{-2})$ for their model during typical storm conditions expected in the field. Using these same arguments, order of magnitude estimates for the above stability parameter in the three-layer model can be calculated and results can be compared to GG. Below z_1 the two models are identical so that the scaling results obtained by GG, which show that z/L is small and can be neglected, also apply to the three-layer model. For $z_1 < z < z_2$ the stability parameter is found by inserting the second equation in (30) into the second equation in (39), giving

$$\frac{z}{L} = \frac{\kappa u_{*cw} z_1}{u_{*t}^4} \sum_{n=1}^{N} g(s_n - 1) w_{f_n} C_{nm}(z_1) e^{-\gamma w_{f_n}(z - z_1)/\kappa z_1 u_{*cw}} \cdot \exp\left[\frac{-\beta w_{f_n}}{\kappa u_{*cw} z_1} \int_{z_1}^{z} \frac{z}{L}\, dz \right]. \tag{40}$$

Inspection of (40) shows that the vertical dependence is controlled by the inverse of a production-related factor $u_{*t}^4/\kappa u_{*cw} z_1$ and two exponential factors. In the transition region all three factors cause the stability parameter to decrease with increasing z. Because the goal is to obtain an upper bound on z/L, the arguments of the exponential terms are set equal to 0. This defines the maximum stability parameter,

$$\left.\frac{z}{L}\right|_{\max} \equiv \frac{\kappa u_{*cw} z_1}{u_{*t}^4} g(s - 1) w_f C_m(z_1) e^{-\gamma w_{f_n}(z - z_1)/\kappa z_1 u_{*cw}}, \qquad z_1 \le z \le z_2, \tag{41}$$

where only one grain size class has been assumed to simplify the discussion. In their scaling analysis, GG adopt values of $\kappa = 0.4$, $z_0 = 0.1$ cm, $g = 980$ cm s^{-2}, $u_{*cw} = 5.0$ cm s^{-1}, $s = 2.65$, $w_f = 1$ cm s^{-1}, and $C_m(z_0) = 1.0 \times 10^{-3}$. In addition, typical values for the following variables must be defined for the three-layer model: $u_{*c} = 1.0$ cm s^{-1}, $\gamma = 0.74$, $\alpha = 0.5$, and $z_1 = 2.5$ cm. Since the stratification correction can only act to reduce further the concentration, inserting the above values into the unstratified version of (30) gives a maximum suspended sediment concentration at $z = z_1$ of $C_m(z_1) = 3.04 \times 10^{-4}$. Using this value for the concentration in (41) translates to a stability parameter estimate of $z_1/L = 3.9 \times 10^{-3}$, which is an order of magnitude smaller than that obtained by GG, who showed that z/L in the wave boundary layer is small and can be neglected. At $z = z_2 = z_1 u_{*cw}/u_{*c}$ the characteristic shear velocity u_{*t} is equal to u_{*c}, so that (41) yields $z_2/L = 2.5$. For the three-layer model used here the stability parameter is O(1) for $z_1 < z < z_2$ and, unlike GG, cannot be neglected in the transition layer. We therefore choose to retain the stability parameter throughout the wave boundary layer in this model. This has implications for sediment transport prediction, where the more idealized eddy viscosity used by GG may artificially reduce the influence of stratification in the wave boundary layer and therefore overpredict the transport for these storm conditions.

2.6. Solution Procedure for the Mean Current and Concentration

The solution for the current and the mean suspended sediment concentration for a stratified bottom boundary layer can now be completely specified given the following set of input variables: $C_{nm}(z_0)$, u_{*c}, k_b, A_b, u_b, and ϕ_{cw}. Because application of this model for the continental shelf requires measurements of the near-bottom flow field to obtain the wave parameters, it is often more convenient to prescribe the mean current u_r at a known height above the bed, z_r, which, for computational purposes, is equivalent to specifying u_{*c}. With this substitution the input variables now become $C_{nm}(z_0)$, u_r, z_r, k_b, A_b, u_b, and ϕ_{cw}, all of which, except for the boundary values k_b and $C_{nm}(z_0)$, are measurable by a single high-frequency current meter/pressure sensor combination. Given these boundary values from other sources, the solution for the coupled boundary layer equations proceeds as follows.

The first step is to determine initial estimates for u_{*c} and u_{*cw}. Because the speed of convergence is generally much faster when the stratification correction is not included, the neutral version is run and the computed values of u_{*c}, u_{*cw}, f_{cw}, and C_R are input into the first iteration of the stratified model. Given these initial estimates, ξ_0 is defined through (24), and ξ and ξ_2 are determined from α and ε, where α is presumed known and $\varepsilon = u_{*cw}/u_{*c}$. The nondimensional length scales ξ_0, ξ_1, and ξ_2 along with ε are substituted into Γ_{cw}, which is solved using the polynomial approximations of the Kelvin functions given by *Abramowitz and Stegun* [1964]. Once Γ_{cw} is known, f_{cw} is determined from (22), which in turn is used to estimate u_{*wm} through (18) and update C_R and u_{*cw} through (17) and (16), respectively. The updated values are then used to recalculate ξ_0, ξ_2, and ε to produce a new friction factor. This inner loop is repeated until u_{*cw} converges. The shear velocities and reference concentration are then used to determine the concentration profile for a neutral ($z/L = 0$) boundary layer. The resulting profile is inserted into (39) to define the stability parameter, which is inserted back into (30) to update the concentration profile. The procedure is repeated until the stability parameter converges. Once the stability pa-

rameter is known, it, along with z_r and the initial guess value of u_{*c}, is inserted into (28) to determine $U(z_r)$. If $U(z_r)$ does not equal u_r, then the procedure starting with the stratified model is repeated with a new u_{*c} until the calculated current equals u_r. Because it is not possible to obtain an algebraic expression for u_{*c} from (28), the solution must be determined iteratively. For this study the secant method is chosen to update u_{*c} because it is rapidly convergent for many nonlinear problems if the initial estimate is sufficiently close to the actual value.

3. Theoretical Model Comparisons and Model Sensitivities

An analysis of nearly 2 years of wave and bottom current data collected at the ~12 m isobath off the southern coast of New Jersey identified 19 storms in 1994 and 1995 [*Styles*, 1998]. Storm activity in 1994 was more frequent and produced generally higher wave heights and bottom currents than activity in 1995. The first storm, recorded in March 1994, produced significant wave heights of 3 m with peak periods of 8.3 s and bottom current magnitudes of nearly 30 cm s^{-1} at a height of 2 m off the bed. Although this first storm was not the largest, it did fall within the top 25% of all the storms on the basis of significant wave height measurements. It is therefore chosen as a representative example of storm conditions that can be expected to occur several times a year for this area.

In addition to wave and bottom current data the bottom boundary layer model requires as input bottom roughness length, sediment reference concentration, and sediment grain diameter. Section 1 mentioned that a number of independent bottom roughness and reference concentration studies have been carried out by other investigators. To incorporate the results of these studies, some of which have undergone further upgrades since they were initially published [*Styles*, 1998], is beyond the scope of this paper. The purpose here, rather, is to introduce the core component of an evolving bottom boundary layer model that will eventually include many of these new features. As an alternative, we have chosen representative values for bottom roughness and reference concentration as produced by GG, which are adequate for this theoretical test.

Surface sediment samples have also been collected at the same location as the wave and current measurements. The results indicate a mixture of mostly medium to fine-grained sand in the 0.01–0.04 cm diameter range. The following series of comparisons were all conducted using several sediment grain diameters over an even broader range. Each case presented here is limited to the grain diameter within the observed 0.01–0.04 cm range that most clearly illustrates the point of the discussion.

3.1. Comparison of Neutral Versus Stratified

In this section, neutral and stratified versions of the three-layer model are driven by the input storm data listed in Table 1 to highlight the significance of the stratification correction. To emphasize the differences between the stratified and unstratified versions of the model, the grain diameter is set equal to 0.01 cm ($w_f = 0.68$ cm s^{-1}). The parameter α is set to a central value of 0.5, which was suggested by *Madsen and Wikramanayake* [1991] for modeling currents in the presence of waves. Further tests of the stratified model will include examining the effects of different grain size classes and sensitivities to α.

Table 1. Input Parameters for Theoretical Model Comparisons

Parameter	Value
Wave	
A_b, cm	79‘
u_b, cm s^{-1}	60
Current	
u_r, cm s^{-1}	29
z_r, cm	200
ϕ_{cw}, deg	24
Sediment/Fluid	
s	2.65
g, cm s^2	981
k_b, cm	30.0
$C_{nm}(z_0)$	0.00280

The stability parameter for the stratified model is presented in Figure 5a; z_1 and z_2 are also shown for comparison. The stability parameter is small in the wave boundary layer, peaks at z_2, and then decays monotonically throughout the outer boundary layer. For the choice of input conditions adopted here the stratification effect is greatest near the top of the wave boundary layer. The associated concentration profile is depicted in Figure 5b along with the profile generated from the unstratified model. The differences in the concentration estimates are striking in the outer layer ($z > z_2$), where stratification (as measured by the magnitude of the stability parameter) significantly reduces the vertical flux of suspended sediment. Without the stratification correction, concentrations at $z = 1000$ cm are only an order of magnitude lower than at the bed. In contrast, concentrations are reduced nearly 4 orders of magnitude for the stratified model. The stratification effect on the mean current (Figure 5c) is nearly opposite to that of the concentration, where the greatest difference between neutral and stratified profiles occurs in the transition region much closer to the bed than the outer region. Most traditional measurements of the bottom boundary layer have been made above the wave boundary layer, where the stratified and unstratified current profiles look similar but where the concentration profiles are different. This implies that while it may be difficult to detect the stratification effect with traditional current measurements, it may be easier to detect it in the concentration observations. The most significant effect of stratification is in the sediment transport,

$$q(z) = C_m(z)U(z), \tag{42}$$

which shows an order of magnitude difference in peak values between the neutral and stratified models (Figure 5d). Total depth-integrated sediment transport

$$Q = \int_{z_0}^{h} q(z)\, dz, \tag{43}$$

where the height h is arbitrarily set to 1000 cm since the contributions to the integral usually become insignificant before reaching this level, is 2 orders of magnitude greater for the unstratified model.

The differences between the two models are also apparent in the u_{*c} estimates, where the neutral model predicts a value of 3.2 cm s^{-1} compared to the lower value of 1.7 cm s^{-1} for the stratified version. Because the time-averaged shear stress is

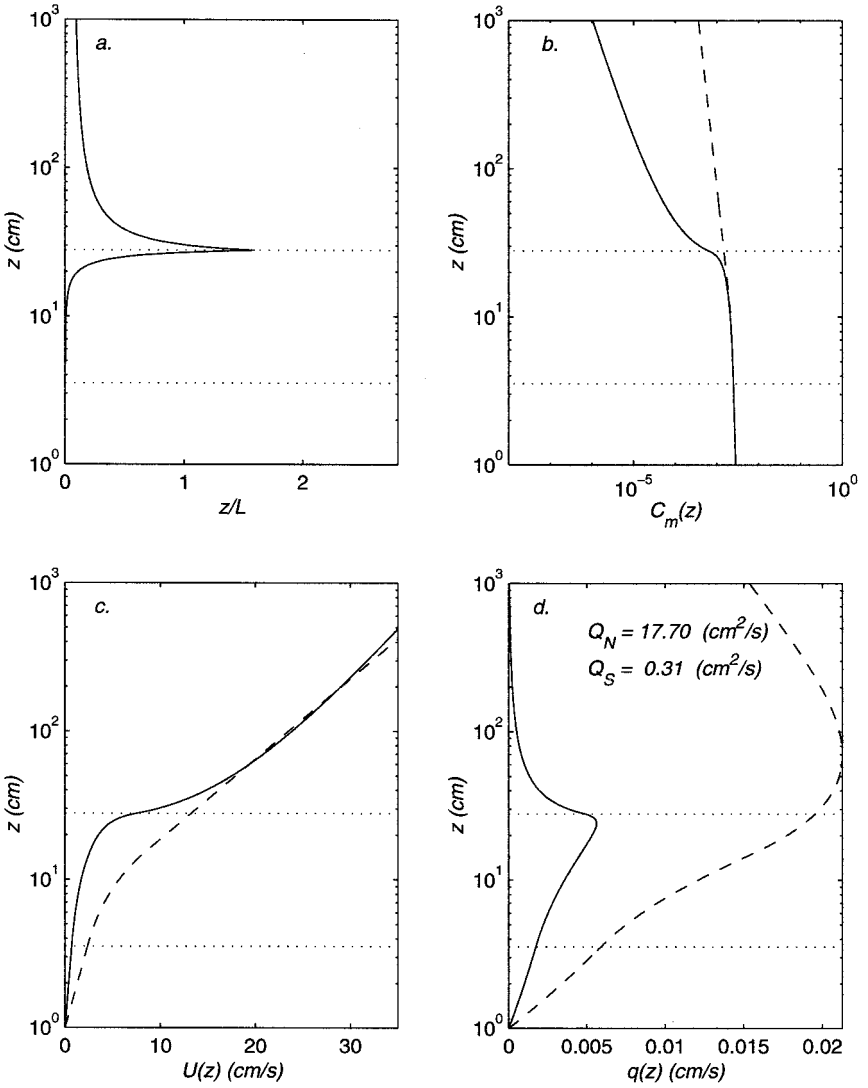

Figure 5. Comparison between the neutral (dashed) and stratified (solid) bottom boundary layer models: (a) stability parameter, (b) suspended sediment concentration, (c) mean current, and (d) sediment transport. Q is the depth-integrated sediment transport defined in (43) for the neutral (N) and stratified (S) models. Horizontal dotted lines denote the heights z_1 and z_2 computed from the neutral model.

proportional to the square of the friction velocity, this result identifies a potentially large source of uncertainty in the momentum balance for the storm-driven shelf currents and will likely influence any predictions derived from a coupled shelf circulation–bottom boundary layer model.

3.2. Comparison With GG

The GG model includes a similar turbulence closure scheme and a correction for suspended sediment–induced stratification but has an eddy viscosity that is discontinuous with only two layers and a stability parameter that is only applied above the wave boundary layer. The storm data listed in Table 1 are used to drive the two models to reveal their quantitative differences. A grain diameter of 0.04 cm ($w_f = 5.62$ cm s^{-1}) is chosen to emphasize the differences between GG and the present model. The free parameter α, which regulates the height z_1, is allowed to vary since it is still relatively unknown for the field. Upper ($\alpha = 1.0$) and lower ($\alpha = 0.15$) bounds are chosen to reflect the values associated with the wave shear velocity sensitivity analysis used to simplify the stability parameter. A middle value ($\alpha = 0.49$) is chosen so that z_2 equals the height of the wave boundary layer computed from the GG model.

Figure 6a shows the stability parameters calculated from the GG two-layer model and this three-layer bottom boundary layer model as a function of height off the bed. Also shown are z_2 and, for comparison, the wave boundary layer height δ_w as calculated from the GG model. The stability parameter computed using the GG model is maximum at δ_w and then monotonically decreases throughout the outer boundary layer. The stability parameters calculated from the three-layer model are small near the bed, peak at or just below z_2, and then rapidly decay above z_2. The peak identified by $\alpha = 1.0$ is smooth, while the peaks for the other two profiles are kinked. Inspection of Figure 4 shows that the approximations (38) for $\varepsilon = 5$ and 10 have a strong kink at z_2 when $\alpha = 0.15$ but are smooth when $\alpha = 1.0$. This behavior is mimicked in the stability parameter profiles depicted in Figure 6a, where the kink is well defined at z_2 for the profiles associated with the lower two values of α.

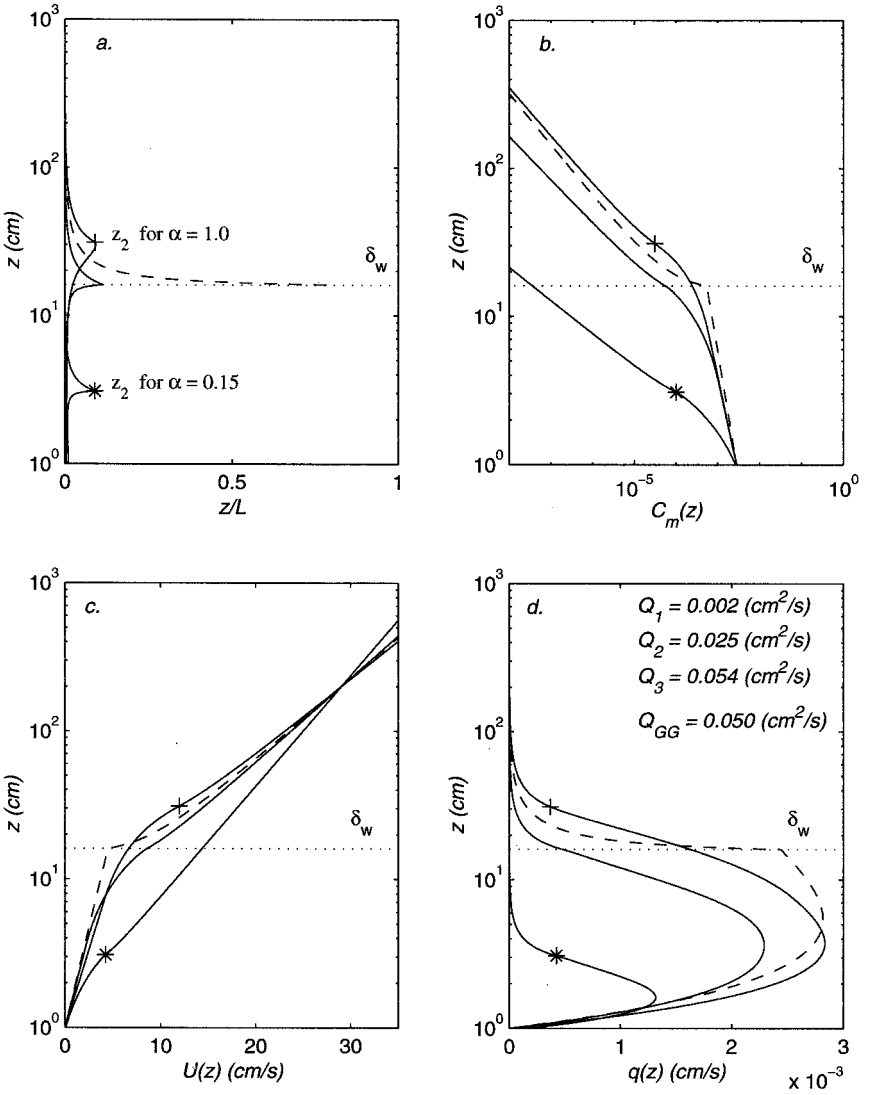

Figure 6. Sensitivity of calculated model profiles to changes in α: (a) stability parameter, (b) suspended sediment concentration, (c) mean current, and (d) sediment transport. Also shown are equivalent profiles calculated from the GG model (dashed) including δ_w for comparison. Asterisks denote z_2 for $\alpha = 0.15$, and pluses denote z_2 for $\alpha = 1.0$. For $\alpha = 0.49$, $z_2 = \delta_w$. Numeric subscripts correspond, in increasing order, to $\alpha = 0.15$, 0.49, and 1.0.

The large differences in peak values provided by GG and the present model are attributed to the assumption on the part of GG concerning the applicable range of the stability parameter (section 2.3) and to the different eddy viscosity configurations.

Figure 6b depicts the concentration profiles. Unlike the smooth three-layer model, the GG model possesses a sharp kink and predicts a higher concentration at the top of the wave boundary layer. This higher concentration is a result of the linearly increasing eddy viscosity, which leads to an increase in the turbulence flux of sediment mass between z_1 and δ_w. The three-layer model uses a constant eddy viscosity in this region that is smaller, so that the sediment flux is weaker. Above δ_w the GG profile has an initial sharp drop in concentration and then a more gradual gradient throughout the outer boundary layer. The sharp drop is a result of the stratification correction (stability parameter) that reduces the sediment flux above δ_w. The reduction in the concentration associated with stratification for the three-layer model is less significant since the stability parameters are smaller. The presence of an artificial kink and the sharp jump in z/L at δ_w, both of which arise from the discontinuity in the GG eddy viscosity, help to rationalize the decision to adopt a more realistic continuous eddy viscosity formulation.

Figure 6c presents the current profiles. Model sensitivities to changes in α are relatively weak for points very near or very far from the bed. The profiles are more sensitive in the region 2 cm $\lesssim z \lesssim$ 100 cm. The GG model produces lower current speeds than the three-layer model at δ_w because of the discontinuous eddy viscosity and the neglected stability parameter in the wave boundary layer. Because most of the suspended load is often carried within the wave boundary layer or just above it, accurate estimates of both the concentration and the current in this region are important for sediment transport studies. This accuracy may be difficult to achieve using the more idealized GG model. To illustrate this point, Figure 6d shows the sediment transport. Regardless of α, the GG and

Table 2. Sediment Transport Q Subdivided According to the Three Regions Defined by the Eddy Viscosity Profile[1]

	$\alpha = 0.15$	$\alpha = 0.49$	$\alpha = 1.0$
$z_0 < z < z_1$	1.75×10^{-4} (7%)	4.70×10^{-3} (19%)	1.64×10^{-2} (31%)
$z_1 < z < z_2$	1.79×10^{-3} (76%)	1.76×10^{-2} (70%)	3.19×10^{-2} (59%)
$z_2 < z$	3.97×10^{-4} (17%)	3.01×10^{-3} (11%)	5.44×10^{-3} (10%)
Total	2.36×10^{-3}	2.53×10^{-2}	5.37×10^{-2}

[1]Units for Q are $cm^2\ s^{-1}$ and $d = 0.04$ cm. Numbers in parentheses indicate percent of total.

three-layer model show larger differences in the current and concentration profiles. This is because the GG model predicts much higher concentrations and only slightly smaller currents near δ_w so that the product generally reflects the greater influence of the concentration. The presence of the kink also causes a sharp drop in transport at δ_w. A smooth profile is more likely to reproduce accurately the details of the sediment transport profile in this region. The depth-integrated transport Q increases with increasing α, and it is in closest agreement with the GG model when $\alpha = 1.0$ instead of when $\alpha = 0.49$. This is a somewhat unexpected result since the latter value of α is chosen to ensure that the wave boundary layer thickness for both models is the same and therefore should produce results that more closely resemble those of the GG model.

A comparison between the two models for $z_2 = \delta_w$ and the same input conditions revealed that the largest differences in Q occurred for grain sizes in the range 0.03–0.05 cm. For grain sizes both smaller (0.01–0.02 cm) and larger (0.06–0.08 cm) than this range the two models began to produce similar Q. The slightly smaller grain sizes have lower settling velocities and lead to a stronger stratification effect (see section 3.3), while the larger grains have a much higher settling rate and produce a negligible effect. When stratification is negligible, both models produce similar concentration and current profiles except in the vicinity of δ_w where the profiles computed from the GG model are kinked. In this region the GG model predicts smaller currents but higher concentrations than the three-layer model, so that the product tends to produce similar sediment transport profiles and hence similar Q. Under these storm conditions, when stratification is very strong, the stability parameter calculated from the three-layer model (see section 3.1) is similar to the GG profile, so that the concentration and current profiles are very similar above z_2 (δ_w). For the inner region and lower portion of the transition region the large turbulent intensity associated with the wave tends to dominate the effects of buoyancy in both models. Therefore, for strongly stratified conditions the sediment transport values and associated Q are similar. Examination of the results depicted in Figure 6 indicates that there is an intermediate range of grain sizes (0.03–0.05 cm) where the GG model produces generally higher Q.

An additional consideration that depends on the eddy viscosity is the distribution of Q between the three layers. This distribution identifies where in the water column the most transport occurs and suggests what regions need to be more closely targeted for modeling and observational studies designed to quantify sediment transport in a combined wave and current bottom boundary layer. To determine what layer carries the greatest transport, the limits on the integral in (43) are divided to correspond with the three layers in the eddy viscosity formulation and the resulting individual transports computed. These integrals are further subdivided according to α, which will affect the distribution of Q by altering the thickness of the individual layers.

The results for these input wave and current conditions are listed in Table 2. In all cases, over 50% of the suspended sediment transport is confined to the transition region ($z_1 < z < z_2$). In fact, for $\alpha = 0.15$ and 0.49 the transition layer carries at least 70% of the total transport. It therefore is especially important to have accurate estimates of the concentration and current profiles (i.e., eddy viscosity) within the transition region for these typical storm conditions. Sediment transport, however, is also a function of grain size, with smaller grains mixed higher into the water column. This could obviously change the vertical distribution of the sediment transport in the bottom boundary layer.

3.3. Sensitivity to α

Using the same grain size, wave, and current parameters as in section 3.1, model results are presented for different values of α. Figure 7a shows the stability parameters. The peaks are an order of magnitude greater than for the 0.04 cm grains (Figure 6a) and are shifted slightly higher along the z axis. The smaller grain sizes have a lower settling velocity that causes a weaker decay in concentration with height. This leads, on average, to higher concentrations and a correspondingly greater potential for a large buoyancy flux near the top of the transition layer where production of TKE by the wave is decreasing. In contrast, the larger grains (Figure 6b) are not mixed as high into the water column so that concentrations at z_2 are generally too weak to produce a large buoyancy flux.

Concentration profiles are shown in Figure 7b. For small z the stability parameter is small and the concentrations do not significantly depart from the log-log ($z < z_1$) or exponential ($z_1 < z < z_2$) variation with height indicative of the neutral model. As the stability parameter becomes larger, the integral terms in (30) become important. This leads to the curvature away from the log-log or exponential behavior in the concentration profiles illustrated in Figure 7b. Higher in the water column, where the stability parameter is again small and stratification is less important, the concentration begins to appear linear when drawn on a log-log axis. The height at which stratification becomes important is also a function of α.

For points below the stability parameter maximum the current (Figure 7c) does not depart significantly from the classic logarithmic ($z < z_1$) or linear ($z_1 < z < z_2$) variation with height indicative of the neutral model. As the stability parameter becomes larger, the current shows a definite upward curvature. This departure from the neutral solution is a result of the stratification correction in (28), which essentially links the effects of buoyancy to the current through the eddy viscosity. The additional influence of α is to further the spread in current values so that at $z = 20$ cm the difference in current speed between $\alpha = 0.15$ and $\alpha = 1.0$ is a factor of about 6. Figure 7d

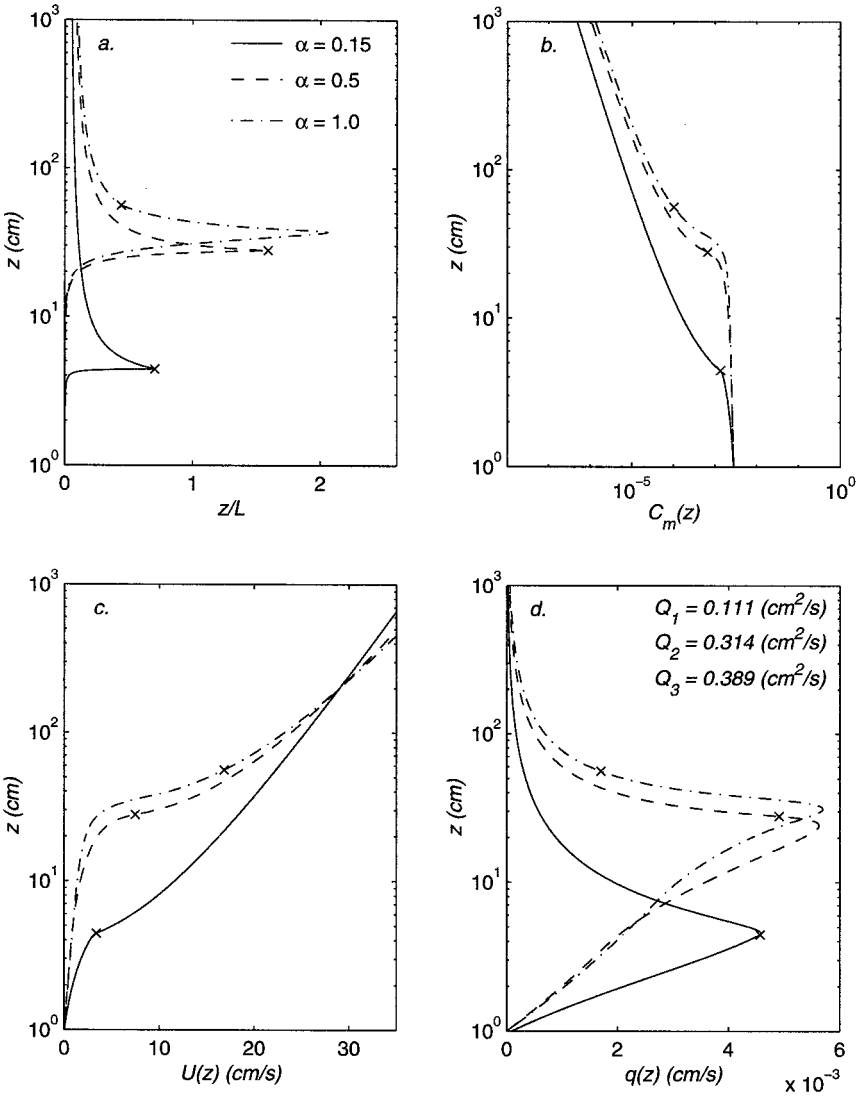

Figure 7. Similar to Figure 5 but for a grain size of 0.01 cm. Crosses mark the height z_2 for each value of α.

depicts sediment transport. Compared to the 0.04 cm grains shown in Figure 6d, maximum transport is greater and is shifted higher along the vertical axis because these smaller particles are more easily lifted higher into the water column and because the stratification correction is not important near the bed. At a height consistent with the stability parameter maximum the transport rapidly decays since the concentration is decreasing at a much faster rate than the current is increasing. The larger transport for the 0.01 cm grains is also reflected in Q, which is an order of magnitude greater than that in Figure 6d. Table 3 lists Q as a function of α for each of the three layers. Unlike for the 0.04 cm grains, the majority of the transport occurs in the outer layer.

3.4. Effect of Increasing the Number of Grain Size Classes

To examine further the stratification effect, the theoretical analysis is expanded to include multiple grain size classes. To keep the analysis relatively simple for this theoretical test, only three grain size classes, 0.01, 0.025 (w_f = 3.01 cm s^{-1}), and 0.04 cm grains, are used. This range represents medium to fine sand, which is expected for typical shallow continental shelves like that observed in the Middle Atlantic Bight off the east coast of the United States. The input parameters are the same as above except that α is set with the intermediate value of 0.5 and the reference concentration is allowed to vary between each grain size class. Assuming a near-Gaussian distribution,

Table 3. Same as Table 2 but for d = 0.01 cm

	α = 0.15	α = 0.5	α = 1.0
$z_0 < z < z_1$	7.09×10^{-5} (<1%)	2.75×10^{-3} (<1%)	1.14×10^{-2} (2%)
$z_1 < z < z_2$	9.81×10^{-3} (8%)	1.06×10^{-1} (35%)	1.85×10^{-1} (48%)
$z_2 < z$	1.02×10^{-1} (92%)	2.05×10^{-1} (65%)	1.93×10^{-1} (50%)
Total	1.11×10^{-1}	3.14×10^{-1}	3.89×10^{-1}

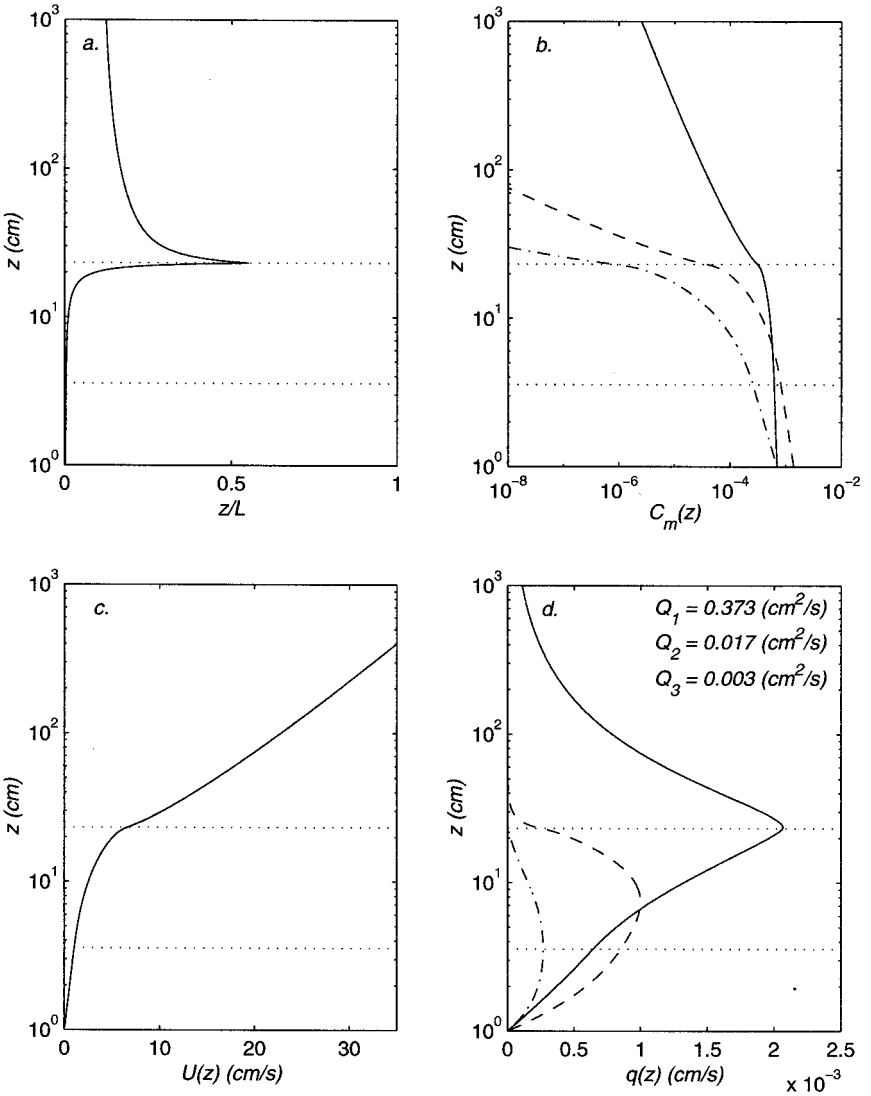

Figure 8. Vertical profiles of calculated model parameters using three different grain size classes consisting of 0.01 (solid), 0.025 (dashed), and 0.04 cm (dash-dotted) grains. The lower horizontal dotted line marks z_1, and the upper dotted line marks z_2. The subscripts on Q indicate in numerical order smallest to largest grains.

the middle grain size class constitutes 50% of the total reference concentration $C_m(z_0) = 2.80 \times 10^{-3}$, and the larger and smaller size classes each constitute 25% of the total.

Figure 8a depicts the stability parameter using the three grain size classes described above. For reference, z_1 and z_2 are also shown. The maximum value depicted in Figure 8a is over twice that shown in Figure 6a, where $\alpha = 0.49$, but only half that shown in Figure 7a, where $\alpha = 0.5$. This indicates that a mixture of heterogeneous sediments that includes the smaller grains, but with a reduced concentration, still leads to a large stability parameter. Sediment concentrations are depicted in Figure 8b. Below z_1, altering the bed concentration distribution leads to an interesting profile structure for these three grain size classes. The medium-sized sediment, although it starts off with the highest concentration in the bed, is barely suspended above the wave boundary layer, rapidly falling out of suspension as the turbulent intensity decreases. The smallest sediment is mixed more uniformly through the water column, so that above the wave boundary layer, it becomes the dominant size class. This illustrates one potential problem with using bed sediment distributions to calibrate sediment concentration sensors. Although not as pronounced, the stratification effect in the current (Figure 8c) is similar to that depicted in Figure 7c, which is based on a single size class consisting of 0.01 cm grains.

Figure 8d shows the sediment transport profiles. The largest grains have a vertical structure similar to that in Figure 6d, and the smallest grains have a structure similar to that in Figure 7d. Near the bed the current is increasing at a rate faster than the suspended sediment is decreasing. The net effect is an increase in sediment transport with distance from the bottom. At points greater than about z_1 the concentration associated with the two largest grain size classes begins to decay, but the smaller grains still have relatively high concentrations. This leads to the decrease in transport for the two larger grains and the continuing increase in transport for the smallest grains. Eventually, concentrations for the smallest grains become so low that the transport must vanish. The differences in the vertical structure for the three grain size classes also is reflected in the value of Q, which varies over 2 orders of magnitude between the

smallest and largest grains. Also, Q for the 0.04 cm grains is an order of magnitude smaller than that shown in Figure 6 for a similar value of α. If Q_3 is adjusted to compensate for the 75% reduction in the reference concentration, it is still less than half that associated with the single grain size class depicted in Figure 5. The influence of stratification induced by the presence of smaller grains causes a greater reduction in concentration for the largest grains than if the smallest grain size class were not present.

Because the parameter γ enters as a constant multiplier of the fall velocity, it produces an effect similar to that of grain size. As a result, sensitivities to this parameter are not presented. It should be noted that the fall velocity is a nonlinear function of grain size. For the examples illustrated here the grain size varies by a factor of 4 (0.01–0.04 cm), with a corresponding variation in fall velocity of an order of magnitude (0.68–5.62 cm s^{-1}). Past work indicates that γ can vary between about 0.35 and 1 [*Hill et al*., 1988; *Villaret and Trowbridge*, 1991; *McLean*, 1992], with a value of 0.74 generally used in applications (GG). Comparisons of the relative changes in γ reported in the past and the fall velocities shown above indicate that the values of d used in this analysis result in greater modulations of the Rouse parameter than equivalent changes in γ. In addition, reductions in γ decrease the Rouse parameter, resulting in larger sediment concentrations higher in the water column. If a smaller γ is applied in conjunction with larger grain sizes, then the larger diameter sediment is lifted higher into the water column where it can stratify the flow. Previous studies [*Styles*, 1998] indicate that setting γ equal to 0.35 with $d = 0.04$ cm produces a stratification effect similar to that associated with the 0.01 cm grains depicted in Figure 5 with $\gamma = 0.74$.

3.5. Sensitivity to β

It has been demonstrated that the model is sensitive to changes in the parameter α. It was also mentioned in section 2 that the numerical value for β, which controls the magnitude of the stratification correction, is derived from experimental studies of stable atmospheric boundary layers. It can be debated that values adopted from atmospheric studies may not be adequate for flows stratified by suspended sediment. In fact, past studies for the atmosphere have shown that β takes on different values under β, stable, or unstable conditions [*Businger et al*., 1971; *Wieringa*, 1980; *Högström*, 1987]. Using values reported in these studies as a guide to investigate sensitivities to this coefficient, β is assigned values of 2, 4.7, and 10, where $\beta = 4.7$ is the value adopted by GG. To preserve continuity with previous sensitivity studies, the wave and current parameters listed in Table 1 will serve for all model runs and α will be set equal to its central value 0.5.

Since β is important in the stratified version of the model, the 0.01 cm grains will be used to enhance the effect of the stratification correction. Figure 9a shows stability parameter profiles for the three indicated values for β. Examination of the profiles reveals an inverse relation, where increases in β correspond to overall decreases in the stability parameter. Figure 9b shows suspended sediment concentration profiles. The three profiles give nearly identical results below about 25 cm where z/L is small but then diverge throughout the remainder of the boundary layer. Interestingly, the profile identified by $\beta = 2.0$, which is associated with the largest stability parameter, shows the weakest decay in concentration with height in the outer boundary layer. This inverse pattern can be explained by examining the exponential term that represents the correction for suspended sediment–induced stratification in the current (28) and concentration (30) equations, i.e.,

$$\exp\left[\frac{-\beta w_{f_n}}{\kappa u_{*cw} z_1}\int_{z_1}^{z}\frac{z}{L}\,dz\right], \qquad z_1 < z < z_2. \tag{44}$$

The stratification correction in both equations depends on the product of β and the integral over the stability parameter. The product $\beta z/L$ is also shown in Figure 9a and generally increases with increasing β. This effectively increases the stratification correction as β becomes larger, but the increase is less than linear because of the corresponding decrease in the stability parameter. This explains why the steepest concentration gradient in the vicinity of z_2 is associated with the smallest stability parameter. This is an interesting consequence since inspection of the stability parameters alone could be interpreted falsely as smaller β producing a larger stratification effect for the typical storm conditions demonstrated here. Examination of Figure 9c shows that the current is not very sensitive to changes in β for the conditions prescribed here. Given the relative insensitivity of the current to changes in β, sediment transport (Figure 9d) profiles follow a pattern similar to that of the concentration, in which the stronger stratification corrections result in less sediment transport. Because the effects of stratification increase in proportion to β, the depth-integrated transport Q decreases with increasing β.

4. Summary

A simple model to describe the vertical variation of the flow and suspended sediment concentration in the constant stress layer above a movable, noncohesive sediment bed has been described. The model predicts mean current and concentration profiles for a fluid stratified by suspended sediment. Closure for the turbulent momentum and mass fluxes was achieved using simple time-invariant eddy diffusivity coefficients modified by a stability parameter to represent the effects of suspended sediment–induced stratification. Like its predecessors [e.g., *Grant and Madsen*, 1979, 1986; GG], this simple turbulence closure scheme was considered appropriate for modeling the constant stress region of the bottom boundary layer and able to describe the first-order effects of turbulent transport in a fluid stratified by vertical concentration gradients in the suspended load. Because of the embedded structure of the wave and current boundary layers, the constant stress layer was divided into an inner region where the maximum stress was a function of the wave and current contributions, a transition region where the wave stress was in a state of decay, and an outer region where the stress was associated only with the time-averaged current.

Expressions for the bed shear stresses were closed using a combined wave and current friction factor that represented the effect of the current through the coupling coefficient C_R. The friction factor was less sensitive to the three-layer eddy viscosity parameters α and ε for smaller relative roughnesses but had a stronger dependence on α for larger roughnesses. Compared to *Grant and Madsen* [1986], the coefficient C_R now depends on three independent parameters (α, ε, and $\mathbf{\Phi}_{cw}$) but was relatively insensitive to the direction between the wave and current for moderate to strong waves as measured by the ratio u_{*cw}/u_{*c}.

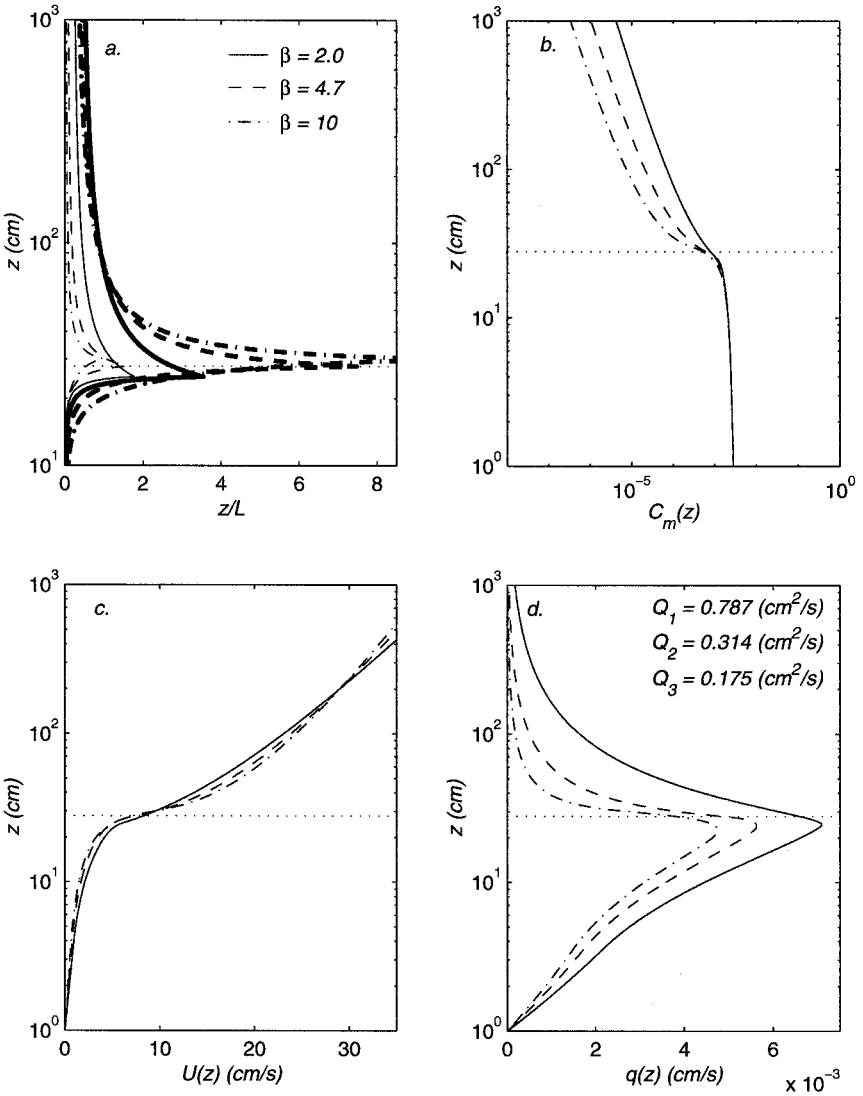

Figure 9. Sensitivity of calculated model parameters to changes in the stratification parameter β. Sediment grain size is set equal to 0.01 cm. The horizontal dotted line marks z_2 calculated with $\beta = 4.7$. The three thicker profiles in 9a are the product of the stability parameter and the corresponding value of β. The subscripts on Q indicate in numerical order smallest to largest β. The vertical scale changes for Figure 9a.

In contrast to the GG model, scaling arguments for the stability parameter in the three-layer model showed that it could not be neglected within the wave boundary layer. In order to ensure that the stability parameter was both continuous and consistent with the definition of the flux Richardson number the production-related term was reevaluated for each of the three layers defined by the eddy viscosity. In the inner layer ($z < z_1$) the shear velocity in the production-related term was equal to the combined wave and current shear velocity evaluated at the bed. To ensure that the production-related term remained continuous, a characteristic shear velocity that had the same functional dependence as the wave shear stress was introduced in the transition region. Above z_2 the stress associated with the wave was negligible, and the shear velocity in the production-related term was equal to u_{*c}.

Comparison between the neutral and stratified versions of the model using data collected on the inner continental shelf offshore of New Jersey showed that the stratification correction can be important during storms. Concentration, current, and especially sediment transport were significantly different between the stratified and unstratified results. Peak transport calculated for the neutral case was over an order of magnitude greater than that for the stratified case. Time-averaged shear velocity estimates derived from the neutral case were nearly twice that of the stratified case.

The model presented here was shown to be more realistic than the GG model in that the current, concentration, and transport profiles were smooth throughout the boundary layer. The stability parameters in the outer layer were very different between the two models except when z was very large and both stability parameters were negligibly small. When compared to the GG model, these profiles were often similar for the current, with greater differences observed in the sediment concentration and transport when the free parameter α was fixed so that $\delta_w = z_2$.

Model sensitivity tests were expanded to include the effects of varying grain size class and closure constants. For the high storm cases presented here, the following were shown.

1. The largest grains considered resulted in the largest differences between the two- and the three-layer eddy viscosity models. Because of the neglect of stratification in the wave boundary layer, the two-layer model produced higher concentrations at δ_w and an unrealistically sharp jump in the stability parameter that artificially capped the wave boundary layer. The three-layer model, on the other hand, produced smaller stability parameters and concentrations and slightly higher currents, so that the transport was lower. This led to smaller depth-integrated transport when z_2 was chosen to coincide with δ_w.

2. The smallest grains within the observed range led to larger stability parameters and to the greatest distortion of the current and concentration from the classic log-linear and Rouse-like profiles derived for the unstratified case. Even though the currents looked similar in the region normally observed, currents close to the bed were very different. Assuming the same reference concentration, differences in suspended sediment concentrations were greatest away from the bed. The resultant transport varied throughout the constant stress region, especially in the most critical part near the bed.

3. Increasing the number of grain size classes produced results similar to the smaller grain size tests. For these conditions the smaller-sized grains significantly contributed to the stratification effect even when they made up only 25% of the bed concentration.

4. The parameter α regulates the structure of the neutral eddy viscosity in the wave boundary layer. Previous comparisons with field and laboratory data produced values of α that varied by a factor of 10. Sensitivities to this level of variation resulted in order of magnitude differences in the depth-integrated sediment transport.

5. The parameter β was more constrained than α, with the expected values varying by only a factor of 5. Increasing β decreased the stability parameter, but the stratification correction depends on their product. The resulting stratification correction for the currents, so long as it is applied, was not very sensitive to the exact value of β within the expected range. Sediment concentrations were more sensitive above the peak in the stability parameter, with larger β reducing the sediment concentration and transport profiles in this region.

6. The parameter γ is the most constrained of the closure constants, with less than a factor of 3 variation in the expected range of values. It controls the Rouse-like decay of the sediment concentration with distance from the bed. Like sediment grain size, decreasing γ increased concentrations and transport throughout the entire water column. It was noted that for larger grains, smaller values of γ resulted in larger sediment concentrations high enough in the water column to stratify the flow.

The sensitivities described above demonstrate the potential of the three-layer model presented here to improve modeling capabilities for currents, suspended sediment concentrations, and transport profiles in the bottom boundary layer during storms on sandy shelves. Both the existing two-layer (GG) and this three-layer model are equally easy to use because they are driven by the same wave and current input parameters, but the three-layer model has the advantage of continuous eddy viscosity and stability parameter formulations. Including the stratification correction in the three-layer model reduces sediment transport estimates by 2 orders of magnitude below that predicted by the unstratified version; however, sensitivities to the closure constants also produce sediment transport estimates that vary by up to an order of magnitude. Observational programs targeted to refine estimates of these closure constants are required to further improve sediment transport estimates.

Appendix A

Grant and Madsen [1979] presented the governing equation for the wave within the wave boundary layer as

$$\frac{\partial u_w}{\partial t} - \frac{\partial u_\infty}{\partial t} = \frac{\partial}{\partial z}\left(K\frac{\partial u_w}{\partial z}\right), \tag{A1}$$

where the horizontal pressure gradient has been expressed in terms of the linearized wave solution evaluated at the bed,

$$u_\infty = u_b e^{i\omega t}, \tag{A2}$$

u_b is the bottom wave orbital velocity, i is the imaginary unit, t is the time, and ω is the wave radian frequency. For convenience the direction of wave propagation has been aligned with the x axis. By defining u_w as the product of a vertical, $f(z)$, and periodic, $e^{i\omega t}$, component, (A1) can be rewritten as

$$i\omega W = \frac{\partial}{\partial z}\left(K\frac{\partial W}{\partial z}\right), \tag{A3}$$

where $W = f(z) - u_b$.

After nondimensionalizing the vertical coordinate (i.e., $\xi = z/l_{cw}$, where $l_{cw} = \kappa u_{*cw}/\omega$) and substituting the eddy viscosity given in (6) the solution to (A3) becomes

$$\begin{aligned}
W &= F(\mathrm{Ber}\ 2\sqrt{\varepsilon\xi} + i\ \mathrm{Bei}\ 2\sqrt{\varepsilon\xi}) + G(\mathrm{Ker}\ 2\sqrt{\varepsilon\xi} \\
&\quad + i\ \mathrm{Kei}\ 2\sqrt{\varepsilon\xi}), \qquad \xi_2 < \xi, \\
W &= Ce^{m\xi} + De^{-m\xi}, \qquad \xi_1 < \xi < \xi_2, \\
W &= A(\mathrm{Ber}\ 2\sqrt{\xi} + i\ \mathrm{Bei}\ 2\sqrt{\xi}) + B(\mathrm{Ker}\ 2\sqrt{\xi} \\
&\quad + i\ \mathrm{Kei}\ 2\sqrt{\xi}), \qquad \xi_0 < \xi < \xi_1,
\end{aligned} \tag{A4}$$

where Ber, Bei, Ker, and Kei are Kelvin functions of order zero [*Abramowitz and Stegun*, 1964] and A, B, C, D, F, and G are complex constants. The nondimensional heights are defined as $\xi_j = z_j/l_{cw}$ $(j = 0, 1, 2)$, and m is defined by

$$m = \frac{1+i}{\sqrt{2\xi_1}}. \tag{A5}$$

The constants are determined by boundary conditions and matching of the solutions in the interior. At the bed, $u_w = 0$, which gives $W = u_w - u_b = -u_b$. As $\xi \to +\infty$, where the limit $+\infty$ is taken in the usual boundary layer sense in that it refers to a distance much greater than δ_w, u_w approaches the solution for irrotational flow so that $W = u_w - u_b = 0$. At the points ξ_1 and ξ_2 the matching condition that the velocity u_w and the shear stress $K\partial u_w/\partial\xi$ be continuous is imposed. Applying the matching and boundary conditions and substituting the definition of W, the general solution for the wave in each of the three layers is

$$\begin{aligned}
u_w &= [u_b + G(\mathrm{Ker}\ 2\sqrt{\varepsilon\xi} + i\ \mathrm{Kei}\ 2\sqrt{\varepsilon\xi})]e^{i\omega t}, \quad \xi_2 < \xi, \\
u_w &= [u_b + Ce^{m\xi} + De^{-m\xi}]e^{i\omega t}, \qquad \xi_1 < \xi < \xi_2, \\
u_w &= [u_b + A(\mathrm{Ber}\ 2\sqrt{\xi} + i\ \mathrm{Bei}\ 2\sqrt{\xi}) \\
&\quad + B(\mathrm{Ker}\ 2\sqrt{\xi} + i\ \mathrm{Kei}\ 2\sqrt{\xi})]e^{i\omega t}, \qquad \xi_0 < \xi < \xi_1,
\end{aligned} \tag{A6}$$

If the flow parameters u_{*cw}, u_{*c}, z_0, z_1, u_b, and ω are specified, the constants in (A6) can be determined from the boundary and matching conditions [*Glenn*, 1983; *Madsen and Wikramanayake*, 1991]. The solutions for the Kelvin functions must be determined numerically, and polynomial expansions, with associated errors for arguments ranging from 0 to ∞, are given by *Abramowitz and Stegun* [1964].

The solution for the wave was derived using the neutral eddy viscosity, and it is important to examine when this approximation is valid for stratified flows. The procedure is to calculate, for a given velocity profile, the change in shear stress that would be caused by the inclusion of the stratification correction and to determine if this change is significant. For this application the shear stresses associated with a given wave velocity profile for neutral and stratified flows are

$$\tau_w = \rho K \frac{\partial u_w}{\partial z} \tag{A7}$$

$$\tau_{ws} = \rho K_{\text{strat}} \frac{\partial u_w}{\partial z}, \tag{A8}$$

respectively, where the subscript ws denotes the modified wave shear stress due to the inclusion of the stability parameter. Dividing both sides of (A7) and (A8) by ρ and subtracting gives

$$\frac{\delta\tau_w}{\rho} = K \frac{\partial u_w}{\partial z}\left[1 - \frac{1}{1 + \beta \dfrac{z}{L}}\right], \tag{A9}$$

where $\delta\tau_w$ indicates the stress difference between the neutral and stratified cases. Near the bed, z is small so that the term in brackets is near zero. At the top of the wave boundary layer the shear for the wave goes to zero, so that the right-hand side of (A9) is small. In both cases, $\delta\tau_w$ is small so that the wave shear stress is described adequately by (A7). While this implies that the stratification correction is negligible for most of the wave boundary layer, it does not preclude an intermediate range where it may have some effect.

Possible stratification effects in the transition layer are estimated by examining the eddy viscosity in (6), which shows that changes in the parameters α and ε that help define z_1 and z_2, respectively, represent arbitrary changes to the neutral eddy viscosity. These arbitrary changes spanned an order of magnitude for α and a factor of 4 for ε resulting in order of magnitude changes in the eddy viscosity in the transition and outer layers. These changes were shown not to affect the wave friction factor solution depicted in Figure 2 except for large roughness configurations. The inclusion of a stability parameter also introduces arbitrary changes to the neutral eddy viscosity. Peak values for the stability parameter, however, are not expected to exceed 10 or so (see section 3). Therefore it is expected that the stability parameter will not affect f_{cw} and associated τ_{wm} unless α and $C_R A_b/k_b$ are small. For small $C_R A_b/k_b$ the roughness will be large, indicating large ripples and low flow velocities. For large ripples and low flow, sediment transport is weak, very little sediment will be in suspension, stratification will be negligible, and z/L will be small. Because the bottom stress is important to the wave and current interaction and is all that directly affects the current, including z/L in the wave solution will not change the results for the current. Therefore z/L in the wave stress calculation is neglected. Because the height of the current boundary layer is much greater than the height of the wave boundary layer, the vertical shear in the current does not vanish until much higher in the water column. This fact suggests that the stratification correction is important for the mean current, except possibly very near the bed where z is small.

The above discussion illustrates an important point about the three-layer eddy viscosity. For large waves (small roughness), suspended sediment concentrations may be large, but the solution for the friction factor is not sensitive to the detailed structure of the eddy viscosity in the outer wave boundary layer. For small waves (large roughness) the solution for the friction factor is sensitive to the three-layer structure of the eddy viscosity, as reflected in the stronger dependence on ε and α. Suspended sediment concentrations, however, are small under these lower wave conditions. Thus the neutral three-layer eddy viscosity is adequate for the wave solution in this application.

Acknowledgments. The first author was funded through the Office of Naval Research/Augmentation Awards for Science and Engineering Research Training (ONR/AASERT) under grant 4-26420. The second author was funded by the Middle Atlantic Bight National Undersea Research Center (MAB 96-10, NYB 94-7) and ONR (N00014-97-1-0797). Both authors were funded by the National Ocean Partnership Program (NOPP) (N00014-97-1-1019 and N00014-98-1-0815) and the National Science Foundation (OCE-95-21102). Institute of Marine and Coastal Sciences contribution number 99-01.

References

Abramowitz, M., and I. A. Stegun, *Handbook of Mathematical Functions*, 1046 pp., U.S. Govt. Print. Off., Washington, D. C., 1964.

Businger, J. A., J. C. Wyngaard, Y. Izumi, and E. F. Bradley, Flux-profile relationships in the atmospheric surface layer, *J. Atmos. Sci.*, *28*, 181–189, 1971.

Drake, D. E., and D. A. Cacchione, Estimates of the suspended sediment reference concentrations (C_a) and resuspension coefficient (γ_0) from near-bottom observations on the California shelf, *Cont. Shelf Res.*, *9*, 51–64, 1989.

Drake, D. E., D. A. Cacchione, and W. D. Grant, Shear stress and bed roughness estimates for combined wave and current flows over a rippled bed, *J. Geophys. Res.*, *97*, 2319–2326, 1992.

Glenn, S. M., A continental shelf bottom boundary layer model: The effects of waves, currents, and a movable bed, Sc.D. thesis, Mass. Inst. of Technol., Cambridge, 1983.

Glenn, S. M., and W. D. Grant, A suspended sediment correction for combined wave and current flows, *J. Geophys. Res.*, *92*, 8244–8246, 1987.

Grant, W. D., Bottom friction under waves in the presence of a weak current: Its relationship to coastal sediment transport, Sc.D. thesis, Mass. Inst. of Technol., Cambridge, 1977.

Grant, W. D., and O. S. Madsen, Combined wave and current interaction with a rough bottom, *J. Geophys. Res.*, *89*, 1797–1808, 1979.

Grant, W. D., and O. S. Madsen, Movable bed roughness in unsteady oscillatory flow, *J. Geophys. Res.*, *87*, 469–481, 1982.

Grant, W. D., and O. S. Madsen, The continental-shelf bottom boundary layer, *Annu. Rev. Fluid Mech.*, *18*, 265–305, 1986.

Hill, P. S., A. R. M. Nowell, and P. A. Jumars, Flume evaluation of the relationship between suspended sediment concentration and excess boundary shear stress, *J. Geophys. Res.*, *93*, 12,499–12,509, 1988.

Högström, U., Non-dimensional wind and temperature profiles in the atmospheric surface layer: A re-evaluation, *Boundary Layer Meteorol.*, *42*, 55–78, 1988.

Jonsson, I. G., and N. A. Carlsen, Experimental and theoretical investigations in an oscillatory turbulent boundary layer, *J. Hydraulic Res.*, *14*, 45–60, 1976.

Keen, T. R., and S. M. Glenn, A coupled hydrodynamic-bottom boundary layer model of Ekman flow on stratified continental shelves, *J. Phys. Oceanogr.*, *24*, 1733–1749, 1994.

Keen, T. R., and S. M. Glenn, A coupled hydrodynamic-bottom boundary layer model of storm and tidal flow in the Middle Atlantic Bight of North America, *J. Phys. Oceanogr.*, *25*, 391–406, 1995.

Lee, T. H., and D. M. Hanes, Comparison of field observations of the vertical distribution of suspended sand and its prediction by models, *J. Geophys. Res*., *101*, 3561–3572, 1996.

Lynch, J. F., J. D. Irish, T. F. Gross, P. L. Wiberg, A. E. Newhall, P. A. Traykovski, and J. D. Warren, Acoustic measurements of the spatial and temporal structure of the near-bottom boundary layer in the 1990–1991 STRESS experiment, *Cont. Shelf Res*., *17*, 1271–1295, 1997.

Madsen, O. S., and P. N. Wikramanayake, Simple models for turbulent wave and current bottom boundary layer flow, *Contract Rep. DRP-91-1*, 150 pp., U.S. Army Corps of Eng., Coastal Eng. Res. Cent., Vicksburg, Miss., 1991.

Madsen, O. S., L. D. Wright, J. D. Boon, and T. A. Chisholm, Wind stress, bed roughness and sediment suspension on the inner shelf during an extreme storm event, *Cont. Shelf Res.*, *13*, 1303–1324, 1993.

McLean, S. R., On the calculation of suspended load for noncohesive sediments, *J. Geophys. Res*., *97*, 5759–5770, 1992.

Nielsen, P., *Coastal Bottom Boundary Layers and Sediment Transport*, 324 pp., World Sci., River Edge, N. J., 1992.

Smith, J. D., Modeling of sediment transport on continental shelves, *The Sea*, vol. 6, edited by E. D. Goldberg et al., pp. 538–577, Wiley-Interscience, New York, 1977.

Sorenson, K. S., O. S. Madsen, and L. D. Wright, Evidence of directional-dependence of moveable bottom roughness in inner shelf waters (abstract), *Eos Trans. AGU*, *76*(46), Fall Meet. Suppl., F281, 1995.

Stull, R. B., *An Introduction to Boundary Layer Meteorology*, 666 pp., Kluwer Acad., Norwell, Mass., 1988.

Styles, R., A continental shelf bottom boundary layer model: Development, calibration and applications to sediment transport in the Middle Atlantic Bight, Ph.D. thesis, Rutgers, The State Univ. of N. J., New Brunswick, 1998.

Traykovski, P., J. D. Irish, A. Hay, and J. F. Lynch, Geometry, migration, and evolution of wave orbital ripples at LEO-15, *J. Geophys. Res*., *104*, 1505–1524, 1999.

Turner, J. S., *Buoyancy Effects in Fluids*, 368 pp., Cambridge Univ. Press, New York, 1979.

Villaret, C., and J. H. Trowbridge, Effects of stratification by suspended sediments on turbulent shear flows, *J. Geophys. Res*., *96*, 10,659–10,680, 1991.

Vincent, C. E., and M. O. Green, Field measurements of the suspended sand concentration profiles and fluxes and of the resuspension coefficient γ_0 over a rippled bed, *J. Geophys. Res*., *95*, 11,590–11,601, 1990.

Wiberg, P., A theoretical investigation of boundary layer flow and bottom shear stress for smooth, transitional, and rough flow under waves, *J. Geophys. Res*., *100*, 22,667–22,679, 1995.

Wiberg, P., and C. K. Harris, Ripple geometry in wave-dominated environments, *J. Geophys. Res*., *99*, 775–789, 1994.

Wiberg, P., and J. D. Smith, A comparison of field data and theoretical models for wave and current interactions at the bed on the continental shelf, *Cont. Shelf Res*., *2*, 126–136, 1983.

Wieringa, J., A revaluation of the Kansas mast influence on measurements of stress and cup anemometer overspeeding, *Boundary Layer Meteorol*., *18*, 411–430, 1980.

Wikramanayake, P. N., Velocity profiles and suspended sediment transport, Ph.D. thesis, Mass. Inst. of Technol., Cambridge, 1993.

Wikramanayake, P. N., and O. S. Madsen, Calculation of movable bed friction factors, *Tech. Rep. DACW-39-88-K-0047*, 105 pp., U.S. Army Corps of Eng. Coastal Eng., Res. Cent., Vicksburg, Miss., 1991.

Wikramanayake, P. N., and O. S. Madsen, Calculation of suspended sediment transport by combined wave and current flows, *Contract Rep. DRP-92-*, 148 pp., U.S. Army Corps of Eng., Coastal Waterw. Res. Cent., Vicksburg, Miss., 1992.

Xu, J. P., and L. D. Wright, Tests of bed roughness models using field data from the Middle Atlantic Bight, *Cont. Shelf Res*., *15*, 1409–1434, 1995.

S. M. Glenn and R. Styles, Institute of Marine and Coastal Sciences, Rutgers–The State University, 71 Dudley Road, New Brunswick, NJ 08901. (styles@deleware.rutgers.edu)

(Received February 16, 1999; revised May 9, 2000;
accepted June 6, 2000.)